

Spring 5-10-2019

# 3D Printed Bioinspired Vascularized Polymers

Kayla Marquis

University of Maine, [kayla.marquis@maine.edu](mailto:kayla.marquis@maine.edu)

Follow this and additional works at: <https://digitalcommons.library.umaine.edu/etd>



Part of the [Biomedical Engineering and Bioengineering Commons](#)

---

## Recommended Citation

Marquis, Kayla, "3D Printed Bioinspired Vascularized Polymers" (2019). *Electronic Theses and Dissertations*. 3040.  
<https://digitalcommons.library.umaine.edu/etd/3040>

This Open-Access Thesis is brought to you for free and open access by DigitalCommons@UMaine. It has been accepted for inclusion in Electronic Theses and Dissertations by an authorized administrator of DigitalCommons@UMaine. For more information, please contact [um.library.technical.services@maine.edu](mailto:um.library.technical.services@maine.edu).

**3D PRINTED BIOINSPIRED VASCULARIZED POLYMERS**

By

Kayla Marquis

B.S. University of Maine, 2017

A THESIS

Submitted in Partial Fulfillment of the

Requirements for the Degree of

Master of Science

(in Biomedical Engineering)

The Graduate School

The University of Maine

May 2019

Advisory Committee:

Caitlin Howell, Professor of Chemical and Biomedical Engineering, Advisor

Douglas Bousfield, Professor of Chemical and Biomedical Engineering

Rosemary Smith, Professor of Electrical and Computer Engineering

# **3D PRINTED BIOINSPIRED VASCULARIZED POLYMERS**

By Kayla Marquis

Thesis Advisor: Dr. Caitlin Howell

An Abstract of the Thesis Presented  
in Partial Fulfillment of the Requirements for the  
Degree of Master of Science  
(in Biomedical Engineering)  
May 2019

Biological vascular systems contain a network of three-dimensional channels that transport and deliver necessary nutrients throughout the organism. These systems are complex, adaptable, and possess the ability to detect and respond to external stimuli as needed. In this work, we mimic the complexity and adaptability of biological systems by incorporating vascular systems into polymeric materials. Vacant channels are created using a fugitive ink technique along with 3D gel printing. Upon completion of vascular channel construction, proof of principle testing is performed by inoculating the polymeric surface with bacteria and adding antibiotics to the vascular channels. The system is then characterized by measuring the resultant areas of inhibition. Computer models are constructed in COMOSL Multiphysics. The vascular system geometry, antibiotic concentration, and effective diffusion coefficients define the model, and are used in conjunction with known bacterial growth parameters such as minimum inhibitory concentration and critical time to determine the final arrangement of bacterial biofilm on the surface. Theoretical models are then experimentally validated. This approach may prove useful in applications such as compact methods of bacterial detection and separation of bacterial multi-cultures based on antibiotic resistance.

## **ACKNOWLEDGEMENTS**

First and foremost, I would like to thank my advisor Dr. Caitlin Howell for introducing me to laboratory research and allowing me to be a part of her lab group. I am so incredibly grateful for the opportunity to have worked with such an enthusiastic and knowledgeable advisor. I also appreciate all of the insightful suggestions and feedback from my committee members Dr. Douglas Bousfield and Dr. Rosemary Smith. Additionally, I would like to thank Dr. Thomas Schwartz who provided valuable feedback on interpretation of modeling data.

I would also like to thank all of my lab team members that have contributed to my project, especially Benjamin Chasse, Anna Webber, and Rachel Detwiler for help with experimental preparation, data collection, and numerous procedural improvements. I would also like to thank Dan Regan for additional help troubleshooting experimental procedures.

The funding for this research was made possible in part by the University of Maine System Research Reinvestment (RRF) grant, start-up funds from the office of the Vice President for Research at the University of Maine, and the Maine Space Grant Consortium Graduate Fellowship Program.

## TABLE OF CONTENTS

ACKNOWLEDGEMENTS .....	ii
LIST OF TABLES .....	vii
LIST OF FIGURES .....	viii
1. INTRODUCTION AND LITERATURE REVIEW.....	1
1.1 Thesis Perspective and Overview .....	1
1.2 Objectives of This Study.....	2
1.3 Literature Review.....	2
1.3.1 Using Stimuli-Responsive and Tunable Surfaces in Biomedical Research.....	2
1.3.1.1 Tissue Engineering Constructs.....	2
1.3.1.2 Smart Materials .....	3
1.3.1.3 Gradient Generators .....	4
1.3.1.3.1 Diffusive Mass Transport.....	6
1.3.2 Microfluidic Device Fabrication.....	7
1.3.3 Conclusions.....	8
2. GENERAL METHODOLOGY .....	9
2.1 Microbial Methodology .....	9
2.1.1 Microbial Strain Information .....	9
2.1.2 Microbial Growth Media .....	9
2.1.3 Microbial Growth Methods.....	10
2.1.3.1 Overnight Stock Solutions .....	10

2.1.3.2 Direct Colony Suspension Method .....	10
2.2 Antibiotics.....	10
3. FABRICATION OF EXPERIMENTAL COMPOUND DELIVERY SYSTEMS .....	12
3.1 Construction of Vascular Systems .....	12
3.1.1 3D Printers .....	12
3.1.1.1 Homemade 3D Printer .....	12
3.1.1.2 Hyrel System 30M Printer .....	12
3.1.2 GCode .....	13
3.1.3 MATLAB GCode Generation.....	14
3.1.4 CAD Files .....	15
3.2 Three-Dimensional Gel Printing.....	15
3.2.1 Agar Platforms .....	15
3.2.1.1 Spatial Control .....	15
3.2.1.2 Temporal Control.....	16
3.2.2 Troubleshooting .....	17
4. CHARACTERIZATION OF VASCULARIZED ANTIBIOTIC DELIVERY SYSTEMS .....	18
4.1 Introduction.....	18
4.2 Materials and Methods.....	19
4.2.1 Inhibition Zone.....	19
4.2.2 Minimum Inhibitory Concentration .....	20
4.2.3 Critical Time .....	20

4.2.4 Evaporation .....	21
4.3 Results.....	22
4.3.1 Inhibition Zone.....	22
4.3.2 Minimum Inhibitory Concentration .....	23
4.3.3 Critical Time .....	24
4.3.4 Evaporation .....	25
4.4 Discussion and Conclusions .....	25
4.4.1 Inhibition Zone.....	25
4.4.2 Minimum Inhibitory Concentration .....	26
4.4.3 Critical Time .....	27
4.4.4 Evaporation .....	27
5. DIFFUSION MODELING OF VASCULARIZED ANTIBIOTIC DELIVERY SYSTEMS .....	28
5.1 Introduction.....	28
5.2 Methods.....	29
5.2.1 Fabrication of COMSOL Model .....	29
5.2.2 Using a Model to Create a Predictive System.....	30
5.3 Discussion and Conclusions .....	33
6. APPLICATIONS OF VASCULARIZED ANTIBIOTIC DELIVERY SYSTEMS.....	35
6.1 Introduction.....	35
6.2 Materials and Methods.....	35
6.2.1 Arbitrary Patterning .....	35

6.2.2 Separation According to Antibiotic Resistance .....	36
6.2.3 Bacterial Regrowth .....	36
6.3 Results.....	36
6.4 Discussion and Conclusions .....	38
7. CONCLUSIONS AND FUTURE DIRECTIONS.....	39
7.1 Review .....	39
7.2 Future Directions .....	39
7.3 Summary .....	40
REFERENCES .....	41
APPENDIX A. VASCULAR CHANNEL CHARACTERIZATION RAW DATA.....	45
APPENDIX B. THEORETICAL MODELING .....	49
BIOGRAPHY OF THE AUTHOR.....	52



## LIST OF TABLES

Table A.1. Inhibition Zone Raw Data.....	45
Table A.2. Minimum Inhibitory Concentration Agar Plate Method Raw Data.....	46
Table A.3. Critical Time Data.....	47
Table A.4. Mann-Whitney U-Test.....	47
Table A.5. Evaporation Data.....	48
Table B.1. COMSOL Model Parameters.....	49

## LIST OF FIGURES

Figure 3.1. Comparison of Homemade 3D Printer and Hyrel System 30M 3D printer.....	13
Figure 3.2. GCode File.....	14
Figure 3.3. CAD File. ....	15
Figure 3.4. 3D Printing Process in Agar. ....	16
Figure 3.5. Spatial Control Patterns. ....	16
Figure 3.6. Temporal Control Pattern. ....	16
Figure 3.7. Fabrication Troubleshooting.....	17
Figure 4.1. Relationship of Critical Time and MIC to Bacterial Growth Curve.....	18
Figure 4.2. Inhibition Zones.....	22
Figure 4.3. <i>E. coli</i> GFP Inhibition Zone. ....	23
Figure 4.4. Minimum Inhibitory Concentration Microplate Broth Dilution.....	24
Figure 4.5. Critical Time.....	25
Figure 4.6. Evaporation.....	25
Figure 5.1. Schematic of COMSOL Simulation Fabrication.....	29
Figure 5.2. Comparison of COMSOL Theoretical and Experimental Results.....	30
Figure 5.3. Process of Creating a Predictive System.....	30
Figure 5.4. Fitting Apparent Diffusion Coefficient to Inhibition Zone, Critical Time and MIC.....	31
Figure 5.5 Surface Concentration for 50 ug/mL Antibiotic Concentration. ....	32
Figure 5.6 Comparison of Theoretical and Experimental Inhibition Zones. ....	33
Figure 6.1. Arbitrary Surface Patterning.....	36

Figure 6.2. Separation According to Antibiotic Resistance.....	37
Figure 6.3. Bacterial Regrowth Following Antibiotic Treatment.....	37
Figure B.1. Standardized Theoretical Inhibition Zones.....	50
Figure B.2. Standardized Theoretical Inhibition Zones.....	50
Figure B.3. Standardized Theoretical Inhibition Zones.....	51

## CHAPTER 1

### INTRODUCTION AND LITERATURE REVIEW

#### 1.1 Thesis Perspective and Overview

Many variations of functional surfaces aimed at achieving a more automated response to various environmental conditions have been established, all with a common goal: achieving greater control over the system. Tunable cell culture platforms have been created to aid in cellular adhesion by simply responding to external stimuli<sup>1-5</sup>. Controlled drug delivery systems have been created to tailor drug release spatially and temporally throughout the body.<sup>6,7</sup> Gradient generators have been created to study the effects of chemical gradients on biological systems *in vitro*.<sup>8-11</sup>

Most recently “smart” materials and surfaces have been created through the inspiration of complex biological systems in nature. Vascular systems, for example contain a network of three-dimensional channels that transport and deliver necessary nutrients and signaling molecules throughout an organism resulting in the ability to detect and respond to external stimuli. Vascular systems have been incorporated in materials to yield highly desirable self-healing<sup>12</sup> and cleaning surfaces.<sup>13</sup> Vascular systems have also been incorporated into various tissue engineering applications. The ability to seamlessly create these vascular channels is attributed to the recent advances in 3D printing technologies.

In this research, vascular systems are incorporated into an agar platform to easily create arbitrarily controlled surface patterning. Our system is unlike current bacterial cell culturing techniques where bioactive compounds are applied onto the agar surface or homogeneously mixed into the agar itself. Using bacteria as a model organism and antibiotics as a bioactive compound, temporal and spatial control of biofilm formation is achievable by coupling our approach with theoretical modeling that allows us to design and predict a priori biological response. Vascular channels are embedded into agar and channels filled with antibiotics of which diffuse to the surface and interact with a biological system.

## **1.2 Objectives of This Study**

The purpose of this work is to create a vascularized bacterial cell culturing platform that is able to control the growth patterns of bacteria at an interface. This platform will control the bacterial coverage on the surface through spatial and temporal control of bioactive compound delivery from the embedded vascular channels to the surface through diffusion. Theoretical modeling will be coupled with experimental results ultimately allowing for behavior prediction of more complex vasculature.

## **1.3 Literature Review**

### **1.3.1 Using Stimuli-Responsive and Tunable Surfaces in Biomedical Research**

The ability to mimic biological conditions *in vitro* is an important step in understanding how a complex biological system operates. By creating compact benchtop systems that closely mimic physiological conditions, researchers gain the ability to study smaller portions of a biological process without the complications of the many other simultaneous processes. First, the creation of specialized materials that are able to mimic these specific biological conditions are necessary. There are numerous applications where materials are tuned to mimic biological systems such as tissue engineering constructs, smart materials, and gradient generators. These applications will be discussed below.

#### **1.3.1.1 Tissue Engineering Constructs**

Vascular channels are essential in complex and multi-layer tissue engineering constructs. This approach may also hold the key to eventual self-repair of injured tissue constructs. Vascular channels are crucial due to their function of transporting blood and necessary nutrients throughout a tissue while removing waste products. Vascular systems are also key in injury repair. Cells must be within 100-200  $\mu\text{m}$  of an oxygen supply to maintain viability.<sup>14</sup> It has been noted that there are significant differences in cell behavior between *in vitro* 2D and 3D culture systems as 3D systems produce much more *in vivo*-like morphologies and behaviors.<sup>15</sup> These observations have led to the incorporation of vasculature into *in vitro* 3D tissue engineering models that are more similar to the actual systems rather than being limited in thickness due to transport limitations.

Common construction methods of the vasculature lumen include micromolding<sup>16</sup> and more recently, 3D printing fugitive ink techniques with materials such as Pluronic F127 (PF127)<sup>13,17</sup>, gelatin<sup>18</sup>, and carbohydrate glass.<sup>19</sup> These vascularized tissue constructs have proven useful in areas including the study of drug delivery and tumors for cancer research<sup>20</sup> as well as the construction of cardiac tissues.<sup>21</sup> The incorporation of vascular systems into biomaterials allows for more dynamic and stimuli-responsive materials.

### **1.3.1.2 Smart Materials**

The development of stimuli-responsive materials has led to a whole new class of materials termed “smart” materials. These materials incorporate surface functionalization or patterning ultimately allowing for the passive response to external stimuli. Examples of smart materials include tunable cell culture platforms, which have been created to aid in cellular adhesion by simply responding to external stimuli, such as heat<sup>1</sup>, light<sup>2</sup>, pH<sup>3</sup>, electric<sup>4</sup>, magnetic fields<sup>5</sup>, and mechanical forces<sup>5</sup>. For example, photoremovable protecting groups of which are attached to the active site of a biomolecule to inhibit activity, can be photocleaved through exposure to light resulting in restored function.<sup>2</sup>

Smart materials in the realm of controlled drug delivery are also of great interest. There are many advantages to a controlled drug release system as opposed to a traditional periodic injection of medication. For example, periodic injections of a drug require administration at specified time intervals. These treatments are only within the effective therapeutic drug concentration window for a period of time and otherwise decrease below this until the next treatment. Controlled released systems on the other hand are able to be tuned so that the release rate matches the elimination rate, eliminating the need for periodic treatments and time below sub-therapeutic drug level.<sup>6</sup> In addition to creating a stable drug profile, these systems can also be tuned to deliver drugs to specific locations by creating pH responsive hydrogels<sup>7</sup>, for example. The incorporation of techniques employed by controlled drug delivery systems provide much promise in the ability to tune bioactive compound delivery in pursuit of next generation stimuli responsive materials.

Some smart materials are inspired by biological systems. For example, vascular systems contain a network of 3-dimensional channels that transport and deliver necessary nutrients and signaling molecules throughout an organism, ultimately resulting in the ability to detect and respond to external stimuli. Vascular systems have been incorporated into materials to yield highly desirable self-healing<sup>12</sup> and antifouling<sup>13</sup> properties. Self-healing surfaces mimic the repair of human skin upon damage using epoxy and its corresponding healing agent dicyclopentadiene (DCPD). When a crack is formed in the epoxy coating, microvascular channels supply the healing agent to repair the crack.<sup>12</sup> Antifouling surfaces employ polydimethylsiloxane (PDMS) with silicone oil inserted into the vascular channels. These self-replenishing vascular systems possess unique surface properties which have been shown to reduce the adhesion of fouling organisms to surfaces without the need for antibiotics or toxic chemicals. Fouling organisms are able to be removed from this fouling-release surface with low hydrodynamic forces.<sup>13</sup> Recent advancements in these stimuli-responsive materials are promising, yet still possess many limitations as they are highly complex and specific resulting in stimuli responses too limited for practical applications.<sup>22</sup> For example, photoremovable groups that inhibit cell adhesion can be photocleaved through exposure to light resulting in restored function; however, this material requires complex chemical reactions to prepare and once photocleavage occurs it is not reversible.<sup>2</sup>

### **1.3.1.3 Gradient Generators**

Chemical gradients and their ability to influence cellular behavior is well established in biology. Examples include embryonic development,<sup>23</sup> inflammatory response,<sup>24</sup> cancer development,<sup>25</sup> and bacterial chemotaxis.<sup>26</sup> Understanding how chemical gradients play a role in the developmental and homeostatic stages of life is very important. Due to the difficulty to isolate processes *in vivo*, devices that generate gradients have been developed for use in benchtop studies.<sup>8-11</sup>

Microfluidic gradient generators are most commonly constructed out of PDMS due to its biocompatibility and oxygen permeability.<sup>27,28</sup> As outlined in a review of microfluidic gradient devices by Kim et al,<sup>9</sup> there are two styles of devices: diffusion and flow-based. Diffusion-based systems rely on diffusive transport to

deliver the molecules of interest to the gradient forming region where as flow-based systems rely on convective transport. A source and sink are used to create a stable and consistent gradient. Flow-based systems may consist of multiple inlets of different solutions that exhibit laminar flow. Diffusive mixing occurs between the solutions as it travels through the microfluidic channels. Flow-based generators are advantageous as they have the ability to rapidly create/change gradient profiles; however, they exhibit many limitations due to the shear stress created by the fluid flow, something that is non-existent in diffusion-based systems.

Flow-based generators are dynamic in nature in that the concentrations and compounds are easily able to be changed. The final outlet gradients can easily be adjusted by simply changing the number, location, and velocities of the inlets. A major motivation for using flow-based generators is their ability to simulate *in vivo* environments where flow-induced shear stresses traditionally occur. Flow-based generators have even made it possible to generate gradients formed through pulsatile release of chemicals.<sup>29</sup> Wound healing assays with tunable cell shear stresses (ideal for mimicking physiological conditions)<sup>30</sup> and chemotaxis assays<sup>26</sup> have also been studied. One disadvantage of these systems is the potential for disruption of normal cellular migration and possible convection influences on migration, making these gradient generator methods only suitable for adherent cell types.<sup>9,28</sup>

Considering the nature of diffusion-based systems they are vastly different from flow-based systems and have the potential for many different applications. They are ideal in cases where convection may cause unwanted shear stress or movement of cells. Depending on the application of this system it may or may not be ideal to have a steady gradient. If a steady gradient is necessary, a source-sink design will need to be used. In designs with static reservoirs unsteady diffusion profiles are generated because as diffusion occurs boundary conditions are altered.<sup>31</sup> The addition of a source and sink will allow for a more controlled and stable gradient.<sup>9,28</sup> The creation of gradient generators has enabled *in vitro* studies investigating cell behavior responses to chemical gradients by mimicking biological gradients with exceptional ability of spatially and temporally controlling chemical gradients.



### 1.3.1.3.1 Diffusive Mass Transport

In order to create a controlled diffusive chemical gradient mass transport must take place through diffusion. Driving forces of diffusion are concentration gradients. When quantifying mass transport, a useful term is the flux. Flux ( $\text{mol m}^{-2} \text{s}^{-1}$ ) quantifies the amount of a material being transported over a given area and time. In cases where additional modes of mass transport such as convection and migration contribute to overall flux, each flux will be summed together to determine the overall flux in the system. The simplest of all cases is Fickian diffusion, it describes solute motion due to concentration gradients. The solute and the material through which the diffusion is occurring have no chemical or physical interactions that may influence the diffusion process.<sup>32-34</sup> In some cases physical changes such as swelling of a hydrogel matrix may also influence diffusion.<sup>7,35-37</sup> Additionally, electrostatic and ionic interactions between species and material of which diffusion is occurring, may be present.<sup>38</sup>

The simplest case of Fickian diffusion occurs when the system is at steady state and the solute concentration does not change over time, this is known as Fick's First Law:

$$\mathbf{N}_i = -D_i \nabla c_i \quad (1)$$

where for species  $i$ ,  $\mathbf{N}_i$  is the molar flux ( $\text{mol m}^{-2} \text{s}^{-1}$ ),  $D_i$  is the diffusion coefficient ( $\text{m}^2 \text{s}^{-1}$ ), and  $c_i$  is the concentration gradient ( $\text{mol m}^{-3}$ ). Using the continuity equation for mass:

$$\frac{\partial c_i}{\partial t} + \nabla \cdot \mathbf{N}_i = 0 \quad (2)$$

where  $t$  is time (s), Fick's first law can be further modified to account for non-steady state diffusion where the solute concentration changes with time, resulting in Fick's Second Law:

$$\frac{\partial c_i}{\partial t} = D_i \nabla^2 c_i \quad (3)$$

Fickian diffusion assumes the diffusion coefficient to be constant at a given pressure, temperature, and material composition.<sup>34,39</sup> For dilute solutions of less than 10% solute concentration dependence is considered negligible.<sup>34</sup>

### 1.3.2 Microfluidic Device Fabrication

Fluidic channels are most often made through molding of PDMS and other polymers.<sup>13,16,40</sup> However, a fugitive ink technique was recently introduced to allow the direct 3D printing of support material in a solid material that is easily removed resulting in vacant channels.<sup>17</sup> Fugitive ink techniques use sacrificial materials during the printing process that can later be removed resulting in vacant channels. Some of the most common sacrificial materials include PF127<sup>13,17</sup>, gelatin<sup>16</sup>, carbohydrate glass<sup>19</sup>, and microcrystalline wax.<sup>41</sup> These materials can be removed from the inside of the matrix material. PF127 can be printed and then removed due to its thermally reversible gelation.<sup>42</sup> At warm temperatures, above 10 °C, the PF127 will gel and as it cools back below 10 °C it will liquefy allowing for removal from a 3D printed vascular network. Gelatin can easily be removed by simply raising the temperature above 37°C.<sup>43</sup>

The most common 3D bioprinting techniques deposit one layer at a time and include inkjet, extrusion, and laser.<sup>44</sup> There are two types of 3D inkjet printing: thermal and acoustic. Thermal inkjet printers heat the print head to produce air pressure pulses forcing droplets from the nozzle while acoustic printers produce pulses from ultrasound pressure or a piezoelectric actuator.<sup>44</sup> Prints can be cured through chemical or photo-crosslinking methods. There are several advantages of inkjet printing including the ability to use liquid or powder support materials. This makes it very simple to remove these materials from the final structure. Inkjet printing also exhibits high printing speeds and a high resolution compared to extrusion and laser printing. Another notable difference between inkjet as opposed to extrusion and laser printers is the low material viscosity range of 3.5-12mPa/s. An example of inkjet printing is the deposition of alginate droplets into a bath of calcium chloride.<sup>43</sup> The calcium chloride bath acts as an ionic cross-linker as well as a liquid support.

Extrusion printing has a mechanical or pneumatic dispensing system that deposits material in a continuous flow. Extrusion printing methods are among the cheapest, simplest, and most versatile. Unlike inkjet and laser printing chemical and photo-crosslinking techniques are not always required and a simple change in temperature may be used.<sup>17,44</sup> The print speed is much slower than both inkjet and laser

printing. Common examples of extrusion printing with fugitive techniques include networks printing in polymeric matrix with PF127<sup>17</sup> and collagen scaffolds with sacrificial gelatin.<sup>45</sup>

Laser printing is significantly less common than inkjet and extrusion most likely due to its complexity. Laser printing has only recently been gaining popularity. Lasers are focused on an absorbing substrate in order to generate pressures that propel printing materials onto a collector substrate.<sup>44</sup> Lasers can also be used for very high resolution polymerization of a monomer solution.<sup>46</sup>

### **1.3.3 Conclusions**

In the recent years there has been much progress in the development of stimuli-responsive and tunable materials. Advancements in 3D printing technologies have allowed for automated fabrication through CAD software with new materials at greater precision and resolution.<sup>44</sup> The development of these materials has allowed for greater ability to simulate *in vivo* environments and mimic physiological conditions. The incorporation of vascular systems into biomaterials has allowed for the creation of 3D culture systems resulting in much more *in vivo*-like cell morphologies and behaviors.<sup>15</sup> Vascular systems have also enabled the transportation of signaling molecules necessary for stimuli-responsive materials.<sup>12</sup> Functionalized surfaces have allowed for response to external stimuli.<sup>1-5</sup> Controlled drug delivery systems enable for customization of drug delivery. Gradient generators have enabled the creation of benchtop models to study the effects of chemical gradients of many biological processes.<sup>23-26</sup> However, there are many limitations with the current stimuli-responsive biomaterial technology. Functional and patterned surfaces are highly complex resulting in stimuli responses to limited for practical applications. Many of these materials also lack the reversibility exhibited in biological systems.<sup>22,47</sup>

## CHAPTER 2

### GENERAL METHODOLOGY

#### 2.1 Microbial Methodology

##### 2.1.1 Microbial Strain Information

The bacterial strains used in this work were *Escherichia coli* K12 W3110 (wild type) CGSC # 4474 obtained from Yale Stock Center, *Staphylococcus epidermidis* 1200 ATCC 12228 obtained from American Type Culture Collection, *Escherichia coli* pBBR MCS-5 (GFP) obtained from Massachusetts Institute of Technology Ribbeck laboratory, and *Bacillus subtilis* MTC 871 (3610*sacA::Phag-mKate2* [KanR] *amyE::PtapA-cfp* [SpcR] *ywrK::PsspB-citrus* [CmR]) provided by the Losick laboratory of Harvard University. Gentamicin resistance is expressed in *E. coli* (GFP) and a resistance to kanamycin is expressed in *B. subtilis*.

##### 2.1.2 Microbial Growth Media

For suspended, liquid-based growth tryptic soy broth (TSB) and Miller's Luria-Bertani (LB) broth were used. TSB and LB were added at a concentration of 0.025 g/mL to DI water. For growth in petri dishes, 0.03 g/mL TSB and 0.015 g/mL bacto agar was used to make tryptic soy agar (TSA) and 0.025g/mL LB and 0.015 g/mL bacto agar to make LB agar. Once mixed, all liquid and agar media were subject to autoclave sterilization at 121 °C for 60 minutes. Once the agar had cooled to touch it was poured into petri dishes. The average volume for square petri dishes was 30mL and the volume for circular petri dishes 25 mL. Once the agar dishes cured, they were stored at 4 °C until used.

When making plates of *E. coli* GFP and *B. subtilis* antibiotics were added following sterilization to select for the antibiotic resistance genotypes. Following addition of antibiotics, the media was subjected to vigorous mixing using a magnetic stir bar and plate.

### **2.1.3 Microbial Growth Methods**

All bacteria were maintained as freezer stocks at -80 °C and grown via quadrant streak plates on either 1.5% Miller's Luria-Bertani (LB) agar or 1.5% tryptic soy agar (TSA) at 37 °C for 18 to 24 hours. Stock cultures were stored at 4 °C for no longer than two weeks before they were re-streaked to avoid contamination and mutations.

#### **2.1.3.1 Overnight Stock Solutions**

Overnight stock solutions were made by adding 3 mL of either tryptic soy broth (TSB) or LB broth to a vented test tube. Approximately 2-3 colonies were taken from a 4 °C stock and transferred to the test tube via sterile wooden applicators and placed in the incubator for 18 to 24 hours. The turbidity of the sample was adjusted by diluting with either TSB or LB to achieve an optical density (OD) of about 0.08 – 0.1 A at 600 nm.

#### **2.1.3.2 Direct Colony Suspension Method**

Isolated colonies were taken from an 18 to 24 hour quadrant streak plate. The isolated colonies were inserted directly into a liquid suspension containing 1x phosphate buffer solution (PBS). The turbidity of the sample was adjusted by diluting with 1x PBS to achieve an OD of about 0.08 – 0.1 A at 600 nm.

## **2.2 Antibiotics**

Antibiotics used in this work include gentamicin sulfate (Sigma-Aldrich G1264) and kanamycin sulfate (Sigma-Aldrich K-4000). Stock solutions of 10 mg/mL of antibiotics were created using sterile DI water and mixing thoroughly with a vortex mixer. Antibiotic stock solutions were stored at 4 °C for no longer than two weeks. When making stock solutions of *E. coli* GFP and *B. subtilis*, gentamicin sulfate and kanamycin sulfate were added at concentrations of 5 µg/mL and 100 µg/mL, respectively.

Gentamicin sulfate and kanamycin sulfate are both broad spectrum aminoglycoside antibiotics which operate by the same mechanism of action: inhibition of protein synthesis. Aminoglycosides bind to the bacterial 30S ribosomal subunit proteins and 16S rRNA, ultimately leading to misreading of mRNA and

incorrect insertion of amino acids into the resulting polypeptide. Due to their interruption of protein synthesis, aminoglycosides exhibit bactericidal activity.<sup>48</sup> It has also been noted that energy is required for the uptake of aminoglycoside antibiotics.<sup>49</sup>

## CHAPTER 3

### FABRICATION OF EXPERIMENTAL COMPOUND DELIVERY SYSTEMS

#### 3.1 Construction of Vascular Systems

##### 3.1.1 3D Printers

###### 3.1.1.1 Homemade 3D Printer

Our homemade 3D printer was assembled by Tom Blough of Wyss Institute at Harvard University and was graciously gifted to the University of Maine Howell laboratory. This printer pictured in Figure 3.1 was used in the early stages of this study; however, it was noted that there were many limitations associated with the use of this printer. This printer had a relatively small printing stage that was only able to move in the XY directions. An independently run syringe pump was used to control the flow of the printing material causing many problems, with the first being that it was extremely difficult to precisely coordinate the movement of the printing bed with the extrusion of the material. Since the syringe pump was not integrated into the printing system itself it was nearly impossible to print designs that were not continuous. The other major problem encountered while using this printer was the inability to control the temperatures of the printer bed, extruder, and the printing environment; temperature control is critical in a pluronic-based printing process, as well as with other temperature sensitive materials. Additionally, this printer was only capable of reading GCodes, meaning more preparation work in preparing a file to be printed. To address these issues the use of more advanced printers was investigated.

###### 3.1.1.2 Hyrel System 30M Printer

The Hyrel System 30M printer was used to 3D print the vascular channels that lie within the compound delivery systems. This printer has many advantages over the homemade 3D printer. With the combination of a completely enclosed printing environment, a heated printing bed, and a variety of specialized temperature-controlled extruders, the printing process was able to be completely temperature controlled. In addition to the temperature-controlled printing environment this printer was also capable of printing in the X, Y, and Z axes. All printing processes (extrusion, printer bed movements, and temperature) were

coordinated with one another allowing for much more complex prints as compared to the homemade printer. This system and its software are capable of reading multiple format types including GCode and STL files. Below a comparison of the two printers discussed can be viewed in Figure 3.1.

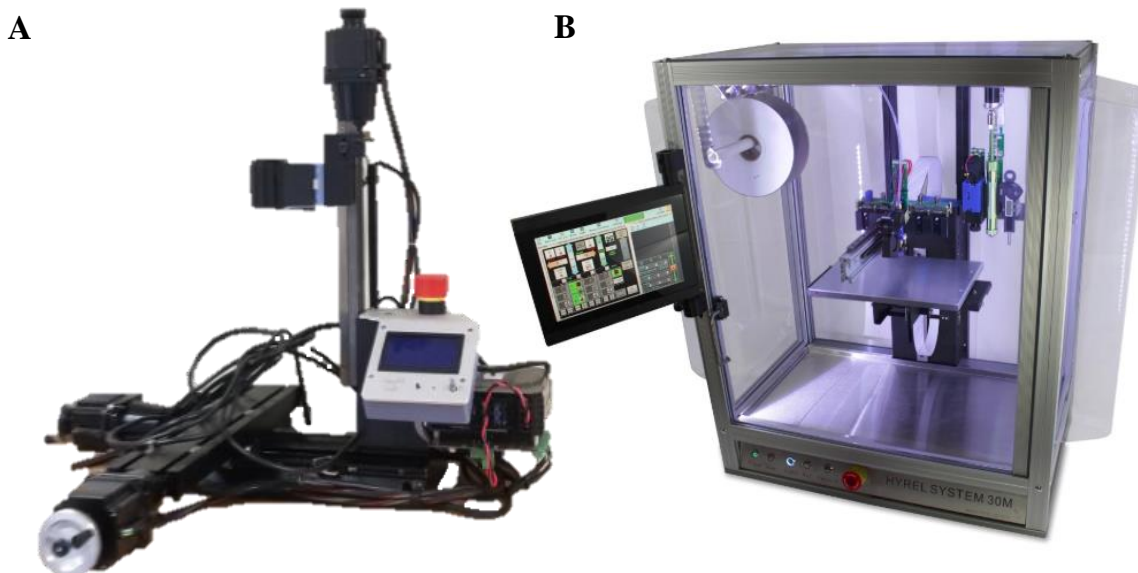


**Figure 3.1. Comparison of Homemade 3D Printer and Hyrel System 30M 3D printer.** (A) The simple and operationally limited homemade 3D printer. (B) the Hyrel System 30M 3D printer which was ultimately used in this study.

### 3.1.2 GCode

A GCode file is a numerical control programming language mainly used for computer-aided manufacturing to control automatic machine tools; in this case, a 3D printer. This file contains all information regarding the print, including printing and non-printing moves and other background information. Printing moves include each individual movement that happens while printing and non-printing moves include times when the extruder is moving, but not printing. Other background information frequently adjusted includes size of extrusion nozzle, printing speed, and temperature. Prior to all printing information lies a printing command, an uppercase letter and number followed by a space. An example of a GCode can be seen in Figure 3.2.



```
10% infill with no skirt - Notepad
File Edit Format View Help
:---
M756 S1.3;
M790 ;execute any new layer actions
;---
G0 Z20;
G0 X96.739 Y111.726 ;
G1 Z0 F1200.000 ; move to next layer (0)
G92 E0 ; reset extrusion distance
G1 X96.739 Y111.726 F1200.000 ; move to first infill point
G1 X96.739 Y52.294 E0.50072 F600.000 ; infill
G1 X111.449 Y52.294 E0.62465 ; infill
G1 X111.449 Y111.726 E1.12537 ; infill
G1 X126.159 Y111.726 E1.24930 ; infill
G1 X126.159 Y52.294 E1.75001 ; infill
G1 X140.869 Y52.294 E1.87395 ; infill
G1 X140.869 Y111.726 E2.37466 ; infill
G0 Z20;
G92 E0 ; reset extrusion distance
M107 T10 ; turn off fans and lasers
G91 ;
G1 Z5.0 ; Drop bed 5mm for extra clearance
G90 ; absolute
G28 X0 Y0 ; home X axis
G92 X0 Y0 ; confirm we are at zero
M84 ; disable motors
M30 ; End ofprogram
; filament used = 4.7mm (1.1cm3)

; avoid_crossing_perimeters = 1
; bed_shape = 0x0,275x0,275x225,0x225
; bed_temperature = 70
```

**Figure 3.2. GCode File.** Printing commands contain an uppercase letter and a number followed by a space and are most frequently at the beginning of each row. Examples of commands are outlined with blue boxes. Printing information such as coordinates (X111.49 Y52.294), amount of material (E0.50072), and printing speed (F1200.000) are outlined in red.

For simple straight-line geometries, GCodes are the preferable file type for printing due to their simplicity. After initial generation of a GCode file that includes printer parameters through the Hyrel software, coordinates can easily be altered for additional geometries. It is important to note that for anything more complex, such as a circle, this method of manually entering coordinates is not practical.

### 3.1.3 MATLAB GCode Generation

When printing line geometry of more complex shapes such as circles or sine-waves a MATLAB code was created to generate the printing move coordinates in an automated fashion.

### 3.1.4 CAD Files

If the desired vascular channel is more complex than that of a single line or equations, CAD files were created using Solidworks. An example of when a CAD file is more convenient to construct than a GCode is when the shape itself is thicker than the extrusion nozzle and will require more than 1 layer.

Following completion of the CAD file it can easily be converted into an STL file, which the Hyrel 3D printer is able to read. STL files are traditionally used for rapid prototyping, 3D printing and computer-aided manufacturing. In order to 3D print it must be used in conjunction with a 3D slicer software – this is built into the Hyrel System 30M printing software. In the 3D slicer, the surface geometry for each individual layer is stored, resulting in a 3D printing process that is performed layer by layer.

Figure 3.3 displays an example of the University of Maine Logo CAD file that was ultimately converted to an STL and printed.



**Figure 3.3. CAD File.** University of Maine logo created in SolidWorks.

## 3.2 Three-Dimensional Gel Printing

### 3.2.1 Agar Platforms

In this research, fabrication methods for two types of systems were developed. The goal of the first system was to achieve spatial control of compound delivery to the surface of the system by varying the placement of the channels. The second, the ability to achieve temporal control of compound delivery to the surface by varying the depths of the channels within the agar itself.

#### 3.2.1.1 Spatial Control

Vascular channels were created by 3D printing 30% (w/v) PF127 channels directly onto the surface of a 100 x 100 x 15 mm polystyrene petri dish at 25°C with a 15-gauge blunt tipped needle. A mass of 35g Miller's LB agar at 4% (w/v) cooled to touch was then poured over the PF127 channels and left to cure at room temperature. Inlet and outlet holes were then melted into the bottom of the petri dish using a 15-gauge blunt tipped needle to allow for removal of PF127. Channels were then rinsed with DI water. With

an  $n$  of 3, the agar thickness was determined to be 3.84 mm with a standard deviation of 0.25 mm. The channels were approximately semicircular in shape with a width of 1.83 mm and height of 1.12 mm with standard deviations of 0.56 and 0.12 mm, respectively. Figure 3.4. demonstrates the printing process. The resultant spatial control patterns of varying complexity achieved through this printing process can be seen in Figure 3.5.

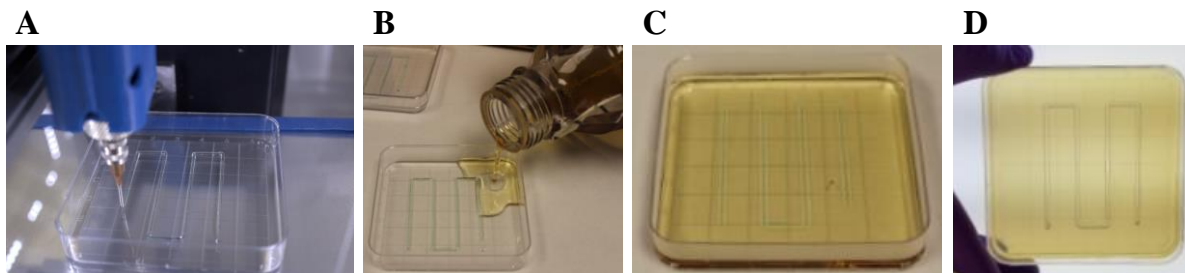


**Figure 3.4. 3D Printing Process in Agar.** (A) vascular Channels are printed directly onto the surface of a petri dish, (B) encapsulation of the vasculature is achieved by pouring liquified agar on top of the gel channel, (C) agar is cured, (D) gel is removed through liquification of the PF127 gel.



**Figure 3.5. Spatial Control Patterns.**

### 3.2.1.2 Temporal Control

By varying the depths of the vasculature within the compound delivery system, temporal control of compound delivery to the surface was achieved. The 3D printing process started off similar to that of the spatial control procedure, the first and deepest channel was printed directly onto the surface of the petri dish using 30% (w/v) PF127. A mass of 35g Miller's LB agar at 4% (w/v) was then poured over the channel and let left to cure half way. Another channel was then printed directly onto the surface of the half-cured agar and then more



**Figure 3.6. Temporal Control Pattern.**

agar poured over the top. This process was repeated until the desired number of channels and thickness of agar was achieved. In Figure 3.6. an image of agar with channels of varying depths can be seen.

### 3.2.2 Troubleshooting

To avoid gaps in the printed channels, it was critical to remove all air from the PF127 prior to printing. This was accomplished by adding the liquified PF127 directly from 4 °C storage into the printing metal syringe and then removing air bubbles by inserting the metal syringe into a vacuum chamber. Next, the syringe was placed in a 70 °C oven for approximately five minutes to allow for gelation. Gelation prior to inserting into the printer is important because this material is prone to foaming when subjected to movement.

PF127 was found to be highly sensitive to temperature differences. For example, when the printing environment was below 10 °C, liquification would occur, resulting in the loss of structural integrity of the channels during the printing process, as seen in Figure 3.7A. Structural integrity of the printed channels

was accomplished by ensuring that on cold days the printer head was set at 25-30 °C and the gel channels were stored in the enclosed printer structure on the heated bed at 30 °C. Another example of loss of structural integrity was observed when the agar used to encapsulate the channels was too hot (Figure 3.7B). In this case, structural integrity of the channels was accomplished with a

lower molten agar temperature. Additionally, it was noted that after pouring the agar over the channels and stacking the dishes to let cure, air bubbles trapped within the PF127 rose to the surface causing openings in the channels. This was solved by letting the dishes cool individually instead of stacking them. Ideally, the agar should be cooled as fast as possible and when the plates were stacked the cooling process was slowed.

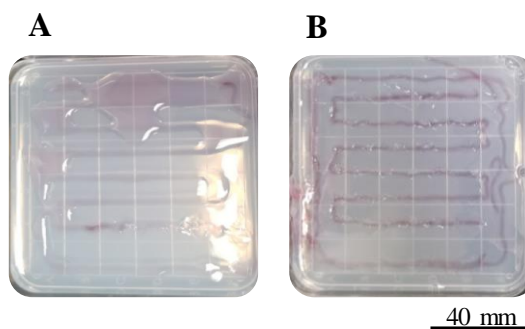


**Figure 3.7. Fabrication Troubleshooting.** Structural integrity loss due to (A) low air temperature (B) too high of an agar temperature.

## CHAPTER 4

### CHARACTERIZATION OF VASCULARIZED ANTIBIOTIC DELIVERY SYSTEMS

#### 4.1 Introduction

Proof of principle testing of the agar-based spatially-controlled antibiotic delivery systems were performed using the bacteria *E. coli* K12 and *S. epidermidis* along with the antibiotic gentamicin sulfate. In order to characterize the system three important parameters have been quantified; inhibition zone, minimum inhibitory concentration, and critical time. The inhibition zone is the distance from the edge of the channels to the point at which bacterial growth occurs visually with the naked eye. The critical concentration at which no bacterial growth occurs is termed the minimum inhibitory concentration (MIC). The time at which the inhibition zone forms is referred to as the critical time. Antibiotics must reach the bacteria prior to the critical time in order for an inhibition zone to be formed. Critical

times will be dependent on a multitude of factors including seed density and growth temperature, for *E. coli* the expected time range should be within three to five hours.<sup>50</sup>

A graphical representation of the relationship

between critical time and MIC to the bacterial growth curve can be seen in Figure 4.1. As depicted in this figure, the critical time occurs soon after the transition from the lag to exponential growth phase, resulting in visualization of growth. Additionally, an inhibition zone will only be present if the MIC is achieved prior to critical time.

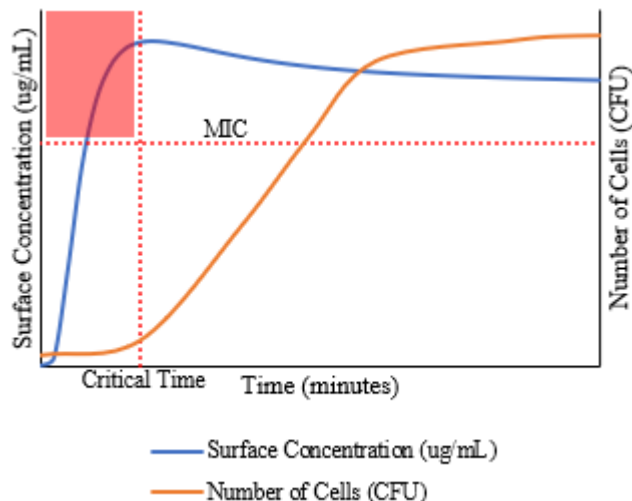


**Figure 4.1. Relationship of Critical Time and MIC to Bacterial Growth Curve.** The red box indicates the time and concentration conditions where no bacterial growth occurs and an inhibition zone is observed.

In this chapter the methods by which the minimum inhibitory concentration (MIC), inhibition zone, and critical time parameters were determined are presented, followed by the interpretation of results. The influence of evaporation on the antibiotics on the channel openings was also investigated.

These methods were created based off of currently accepted techniques published by the Clinical Laboratory Standards Institute (CLSI). Inhibition zone test method ideas were taken from the published Kirby-Bauer disk diffusion test methods, which enable researchers to determine the level of antibiotic susceptibility of individual organisms. This test used a standard Mueller-Hinton agar plate streaked for confluent growth. Six-millimeter filter paper disks impregnated with antibiotics were placed onto the surface of the agar and placed in an incubator for 16 to 18 hours at 35 °C. The inhibition zone diameter was measured from edge to edge and rounded up to the nearest millimeter. Performance standards published by CLSI can then be used to determine the susceptibility, either resistant, intermediate, or susceptible.<sup>51,52</sup> The final parameter of interest in antibiotic susceptibility testing is the minimum inhibitory concentration (MIC), the concentration of antibiotic at which visible growth of the bacteria of interest is inhibited. This parameter is used to determine if a pure culture has been contaminated or has experienced mutations from the wild type.<sup>53</sup>

## **4.2 Materials and Methods**

### **4.2.1 Inhibition Zone**

First, multiple agar vascular channel systems were prepared according to the procedures described in Chapter 3. Agar plates were streaked for confluent growth with a single bacterial species using a sterile cotton tipped applicator. The lid was then placed on the petri dish and it was flipped over so that the channel inlets and outlets on the bottom of the dish were facing up. Various concentrations ranging from 20 µg/mL to 100 µg/mL antibiotics were prepared. Lastly, the antibiotics were added to the channels using a pipettor. Each plate received a different antibiotic concentration so that a dose response curve could be constructed. The plates were incubated at 37 °C overnight for approximately 18 to 24 hours. These plates were photographed and imported into ImageJ where the measurements were taken. The

inhibition zone was determined by measuring the distance between the edge of the channel and the inhibition zone. At least ten measurements were taken for each channel measured.

#### **4.2.2 Minimum Inhibitory Concentration**

Two methods were used to determine the MIC. The original method used for determining MIC was the agar plate method. Here, 1.5% agar was prepared and following sterilization the agar was divided into various 25 mL aliquots. Each aliquot was dosed with a different concentration of antibiotic and thoroughly mixed using a magnetic stir bar and plate. The agar aliquots were then poured into their respective petri dish and left to cure. The plates were then streaked for confluent growth with bacteria using a sterile cotton tipped applicator and placed at 37 °C for 18 to 24 hours. The MIC was determined by identifying the plate with the lowest concentration of antibiotic that was found to completely inhibit the growth of the bacteria.

The second method used was the microplate broth dilution. For this method a 96 well plate is used. Each well contained equal volumes (50  $\mu$ L) of antibiotic, bacterial growth media, and an overnight stock solution of bacteria. Varying concentrations of antibiotics were added to each well. The OD at 600 nm was then recorded. Following the first OD reading, the 96 well plate was incubated on a shaker for approximately 18 to 24 hours. Following incubation, the OD was taken again. The difference in OD was then obtained by subtracting the initial OD from the final OD. The antibiotic concentration that results in a difference of zero, resulting in no bacterial growth, was identified as the MIC. The MIC was measured for *E. coli* wt, *E. coli* GFP, and *S. epidermidis*. Each MIC experiment was performed in triplicate. Two controls were included in these experiments. The first control had growth media, bacteria and PBS which was in place of the antibiotics. The second control contained only growth media and PBS which was substituted in place of the bacteria and antibiotics.

#### **4.2.3 Critical Time**

Agar plates were streaked for confluent growth with a single bacterial species using a sterile cotton tipped applicator. The lid was placed on the petri dish and it was flipped over so that the channels and their inlet

and outlets were facing up. Plates were labeled 1 to  $n$  (the number of total plates, at least 5). A concentration of 50  $\mu\text{g/mL}$  gentamicin antibiotic was added to the channel(s) of plate 1 and the time was recorded. All plates were then placed in the incubator at 37 °C. The total number of plates were divided up by approximately 6 hours. At the calculated time increment, plate 2 was removed from the incubator and 50  $\mu\text{g/mL}$  gentamicin antibiotic was added to the channel(s) and then the plate placed back into the incubator. Time of antibiotic addition recorded was recorded. This procedure was repeated until antibiotics were added to all plates. The plates were stored in the incubator for a total of 18 to 24 hours. Upon completion of incubation, photos were taken of the inhibition zones which were then measured in ImageJ.

The determination of critical time was achieved through plotting the inhibition zone squared against the preincubation time and then identifying the x-intercept of the corresponding linear regression line. This method, published by Cooper and Woodman<sup>54</sup> assumed a linear diffusion gradient and a constant antibiotic concentration and is based off of the following derived approximation:

$$\ln\left(\frac{C_0}{C}\right) = \frac{1}{4DT} y^2 \quad (4)$$

where  $y$  is the distance from the reservoir (mm),  $C$  is the concentration ( $\mu\text{g/mL}$ ) at distance  $y$ ,  $C_0$  is the concentration in the reservoir ( $\mu\text{g mL}^{-1}$ ),  $D$  is the diffusion coefficient ( $\text{mm}^2 \text{hr}^{-1}$ ), and  $T$  is the elapsed time in hours. For the experiments presented in this thesis, this same relationship was assumed to be true. It is possible that the differences of an emptying reservoir altered the squared relationship, however the differences were assumed to be negligible as the concentration gradient that affected the bacteria occurred within the first few hours prior to the channels emptying.

#### **4.2.4 Evaporation**

In order to determine if evaporation was influencing the action of the antibiotics three identical plates, each with three channels, were constructed. The plates were all streaked for confluent growth with *E. coli* K12 and antibiotics of the same concentration were added to all of the channels. Each channel of the plate

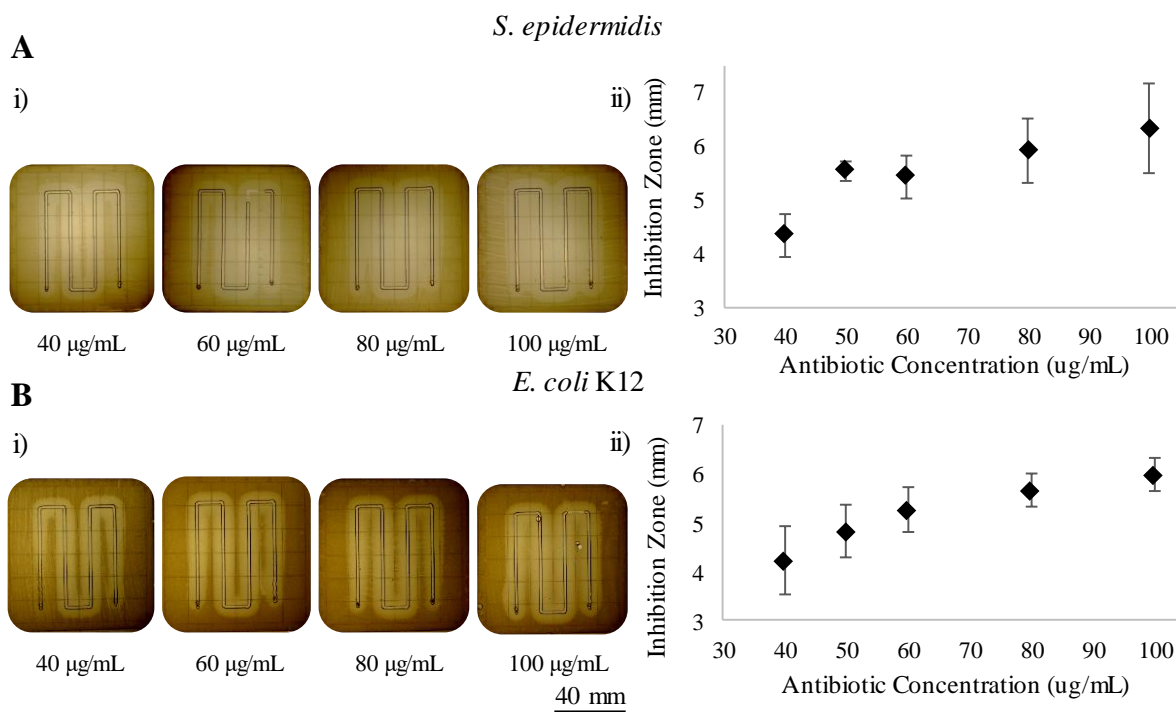


underwent a different treatment following addition of the antibiotics. For treatment 2G, both the inlet and outlet were sealed off with vacuum grease. For treatment 1G, one of the inlet/outlet holes was sealed with vacuum grease. For the third treatment, 0G, the inlet and outlet were left open. The plates were then incubated at 37 °C overnight for 18 to 24 hours. Following completion of incubation, the plates were imaged and the inhibition zones measured in ImageJ. Twenty measurements were taken for each channel.

### 4.3 Results

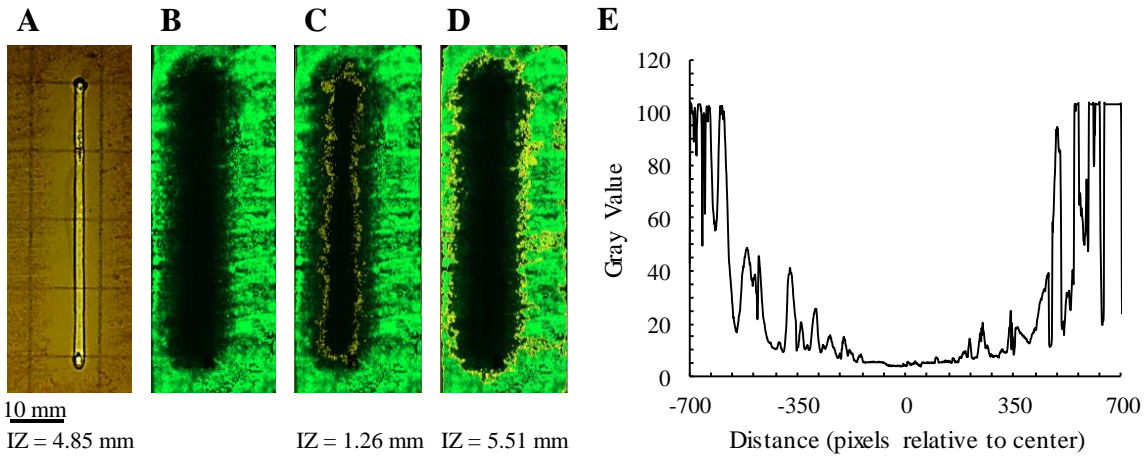
#### 4.3.1 Inhibition Zone

Figure 4.2 shows the relationship between observed inhibition zone at varying antibiotic concentrations. The observed dose-response relationship followed a distinct logarithmic relationship. Four replicates were performed for *S. epidermidis* and six for *E. coli K12*. A table of the individual averages for each concentration and its corresponding standard deviation can be found in Appendix A.



**Figure 4.2. Inhibition Zones.** (A) *S. epidermidis* and (B) *E. coli K12* where i) displays inhibition zones observed at varying antibiotic concentrations from channel side down and ii) dose-response curve generated from the inhibition zone data following addition of a finite volume of antibiotics.

In Figure 4.3 the inhibition zones as seen by the unaided eye and with fluorescence microscopy of *E. coli* GFP can be seen. The inhibition zone from image A) measured by the unaided eye is 4.85mm, C) microscopy image with low threshold was 1.26 mm and D) microscopy image with high threshold was 5.51 mm.



**Figure 4.3. *E. coli* GFP Inhibition Zone.** (A) Results from unaided eye with inhibition zone of 4.85mm, (B) results from fluorescence microscopy, (C) superimposed yellow border of a software generated low threshold inhibition zone measured to be 1.26 mm, (D) superimposed yellow border of a software generated high threshold inhibition zone measured to be 5.51 mm. (E) Gray scale values of image B from left to right of image.

#### 4.3.2 Minimum Inhibitory Concentration

Experiments performed using the agar plate method yielded inconsistent results despite numerous replicates; the raw data can be found in Appendix A. Figure 4.4 shows the results from the microplate broth dilution MIC experiment. The graph displays the difference in OD from the start, when the bacteria and antibiotics are added, to the end following 18 to 24 hours of incubation. An OD difference of zero indicates no bacterial growth. Experimental results indicated that the MIC for *E. coli* K12 was 1.5 ug/mL and *E. coli* GFP, 4 ug/mL. The MIC results for *S. epidermidis* were inconclusive. The controls indicated contamination as there shouldn't have been growth.

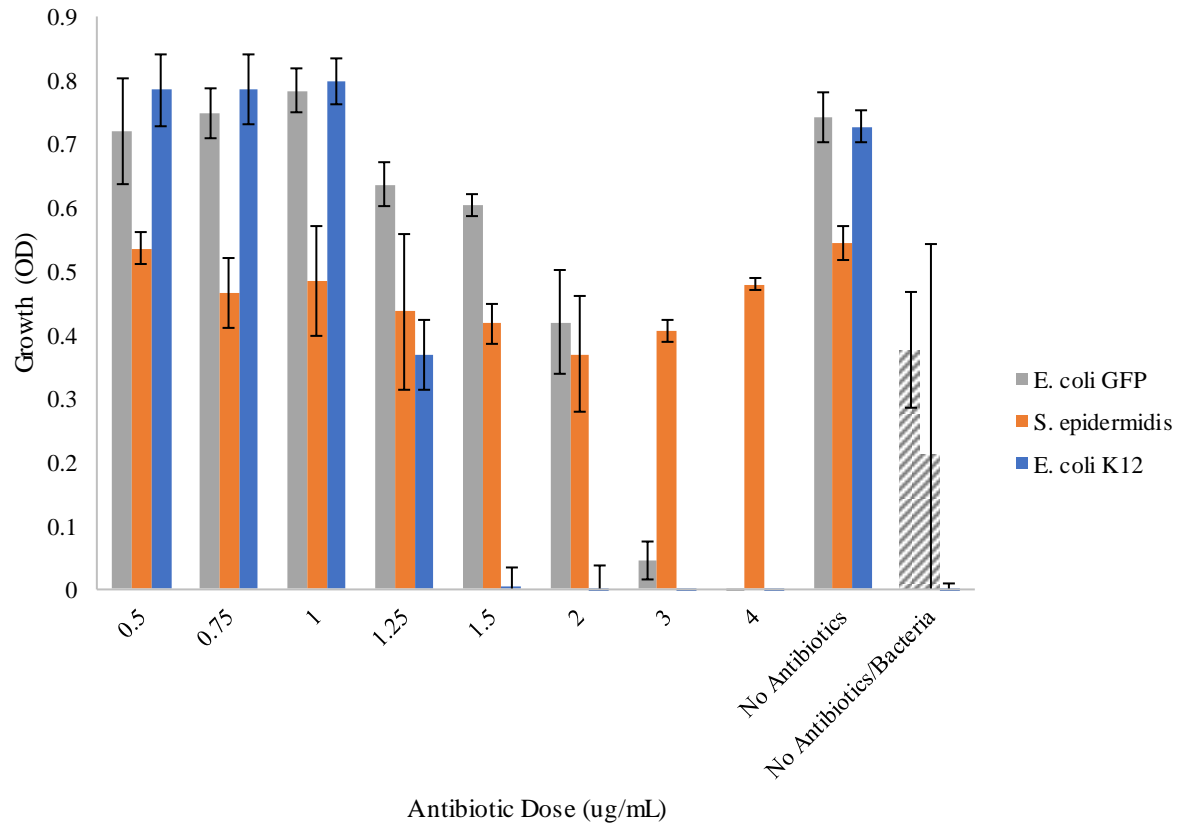


**Figure 4.4. Minimum Inhibitory Concentration Microplate Broth Dilution.** Growth (change in OD) of *E. coli* K12, *S. epidermidis*, and *E. coli* GFP. The gray stripes represent the controls without bacteria.

### 4.3.3 Critical Time

To reiterate, the critical time was the time at which the antibiotics were required to reach the bacteria in order for a distinct inhibition zone to be formed. The Five replicates of the critical time experiment were conducted for *S. epidermidis* and *E. coli* K12. The average critical times for *S. epidermidis* and *E. coli* K12 were 363 and 343 minutes with standard deviations of  $\pm 50$  and  $\pm 37$  minutes, respectively. Figure 4.5. shows the results of a single critical time experiment. With the inhibition zone squared vs. the time at which the antibiotics were added to the plates. A linear function was fit to the data to extrapolate the x-intercept, which indicated the critical time at which the addition of antibiotics did not influence the inhibition zone. Data from each individual trial and bacterial strain can be found in Appendix A.

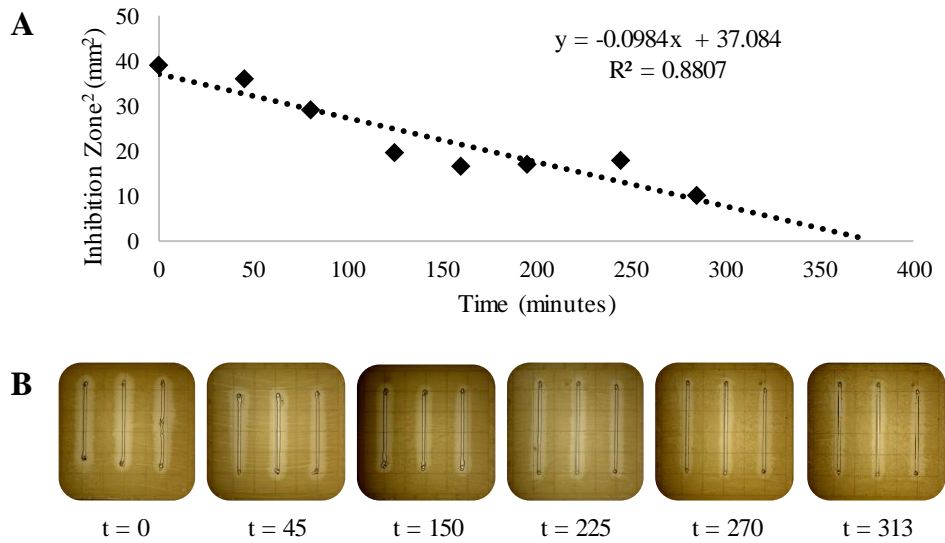


**Figure 4.5. Critical Time.** (A) Graph used to determine critical time and (B) observed inhibition zones of *E. coli* K12.

#### 4.3.4 Evaporation

Using the Mann-Whitney U-test in Minitab software, it was concluded that with 95% confidence there was no statistical difference between the median inhibition zones of the channels with the different treatments (Figure 4.6). Raw data and P values can be found in Appendix A.

### 4.4 Discussion and Conclusions

#### 4.4.1 Inhibition Zone

Dose response curves were successfully generated for *S. epidermidis* and *E. coli* K12 with acceptable standard deviations, especially when taking into consideration the relatively large variation inherent in biological systems. To get a better understanding of the inhibition zone, the differences in the zones from the unaided eye and fluorescence microscopy of two varying thresholds must be further investigated.

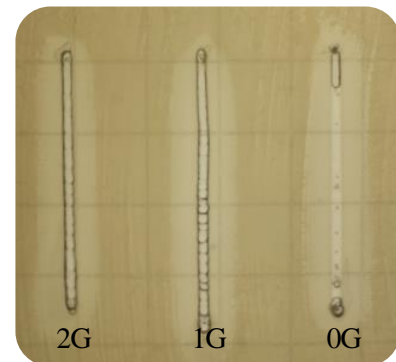


**Figure 4.6. Evaporation.** 2G indicates grease sealing both inlet and outlet, 1G indicates sealing one, and 0G none.

#### 4.4.2 Minimum Inhibitory Concentration

The results from the agar plate method were inconsistent despite numerous replicates and improvements upon the experimental procedure. Initially, inconsistencies were believed to be due to the insufficient mixing of the antibiotics in the molten agar itself, but upon improving the mixing procedure results remained the same. Another idea was that the heat of the molten agar itself was affecting the antibiotics, but after confirmation from manufacturers and literature it was determined that antibiotic effectiveness is very minimally altered even when subjected to very high temperatures experienced during the autoclave process, which is much greater than the temperature of the agar that was being mixed with. After carefully analyzing the colony forming unit (CFU) counts at various antibiotic concentrations from the agar plate method, it was noted that the CFUs that were counted were all relatively small counts as compared to the initial starting concentration on the order of magnitude of  $10^8$  CFU/mL with an estimated amount of  $5 \times 10^6$  CFU/mL transferred from the swab to the plate. Most observed CFU counts were far less than 100, an extremely small fraction compared to the starting CFU counts. These consistently small counts may be attributed to probability. The sensitivity of this method indicated that this method may not be the best option to use in this circumstance.

The results from the microplate dilution method proved to be just as inconsistent from trial to trial. A few explanations for the variation were that when the initial OD is taken the liquid within the plate is homogeneously mixed, but after incubating there are bacterial clumps present when incubated with the shaker. The clumps were attempted to be broken up using a vortex mixer but resulted in splashing between wells. In order to get more consistent results from this experiment, different equipment will be needed such as covers for the 96-well plates and a shaker incubator more suited to a 96 well plate. The reason for using two different methods to measure MIC was to ensure that both methods arrived at the same conclusions, however; this was not the case.

To complicate matters even more the MIC from literature of *E. coli* ATCC 25922 is approximately 0.5 ug/mL of gentamicin.<sup>55</sup> The experimental results yielded values much higher. Due to

all of the inconsistencies it was determined that the MIC values published in literature will be used for further analysis in order to complete modeling in Chapter 5.

#### **4.4.3 Critical Time**

The critical times calculated were roughly 6 hours, within the expected values of 4 to 10 hours described in literature.<sup>56,57</sup> However, upon further investigation it was determined that the critical times discussed in literature applied antibiotics to a disk and placed the disk on the surface of the agar where the antibiotics diffused onto the surface. Our experiments added antibiotics to channels which then had to diffuse through the agar matrix before reaching the surface. Ultimately, it was determined that this difference in experimental setup led to incomparable results. We must use alternate methods to interpret these results.

#### **4.4.4 Evaporation**

It was concluded that there was no statistical difference between the inhibition zone observed with the open channels which experienced evaporation and the sealed off channels where the liquid remained in the channels. The remaining liquid in the channels did not appear to have an effect on the inhibition zone indicating that the remaining liquid in the channels was not the antibiotic solution added at the start of the experiment. It is evident that the antibiotics diffused into the agar matrix independently of the solvent.

## CHAPTER 5

### DIFFUSION MODELING OF VASCULARIZED ANTIBIOTIC DELIVERY SYSTEMS

#### 5.1 Introduction

Here, we explore the use of COMSOL Multiphysics modeling to calculate the mass transport of antibiotic compounds through a bioinspired vascularized polymer system and use this model to predict the growth pattern of a bacterial biofilm on the surface of the polymer. Vascular system geometry, antibiotic concentration, and diffusion coefficient define the model, and were used in conjunction with known bacterial growth parameters such as minimum inhibitory concentration (MIC) and critical time to determine the final arrangement of the biofilm on the surface. The theoretical models were then validated by comparing to experimental results.

COMSOL Multiphysics was used to calculate the concentration field of a solution throughout the diffusion process and displayed an interactive graphical solution. COMSOL is capable of solving stationary and time dependent problems in all space dimensions, but for this application a time dependent solver was used along with the transport of diluted species module. When solving this module COMSOL assumed that the solution was greater than 90% solvent concentration and that the mixture properties (density and viscosity) were of the solvent. COMSOL takes into account three driving forces of transport: diffusion, convection, and migration. However, for this case diffusion was the only factor. In order to calculate the concentration fields COMSOL used Equation (1), Fick's First Law in conjunction with the mass balance equation:

$$\frac{\partial c_i}{\partial t} + \nabla \cdot (-D_i \nabla c_i) = R \quad (5)$$

where  $R$  equals the production or consumption rate expression.

COMSOL used finite element analysis to solve the simulation. This method approximated partial differential equations that are unable to be solved analytically. First, finite element mesh refinement was performed. The CAD model was divided into smaller domains (elements), the smaller the elements, the more refined the mesh and the closer the approximation were to the true solution. Next, the finite element

method was performed. This method took all the partial differential equations for each individual element created in the mesh and solved.

## 5.2 Methods

### 5.2.1 Fabrication of COMSOL Model

CAD files of the vascularized polymeric platforms are created in SOLIDWORKS and exported to COMSOL Multiphysics using the LiveLink feature. For the 3D printing process, a 15-gauge needle (approximately 1.3 mm inner diameter) was used to print the PF127. However, the channel does not remain circular upon coming into contact with the petri dish. To determine the actual shape of the channel needed to be designed in SolidWorks, cross-sectional areas were cut from constructed vascular systems and measured. Here a semicircular channel shape of radius of 0.9 mm was used.

In COMSOL a simulation was created using the transport of diluted species physics in a time dependent solver. The model assumed Fickian diffusion and therefore a constant diffusion coefficient. The simulation inputs included diffusion coefficient and antibiotic concentrations in both the channels and the surrounding agar. A no flux boundary condition for all surfaces of the agar was also initiated. Simulation outputs included concentration vs. time profiles (Figure 5.1). Instead of inputting the known diffusion coefficient of gentamicin and 4% agar, the apparent diffusion coefficient which takes into account for the biological aspects of the system was inputted.

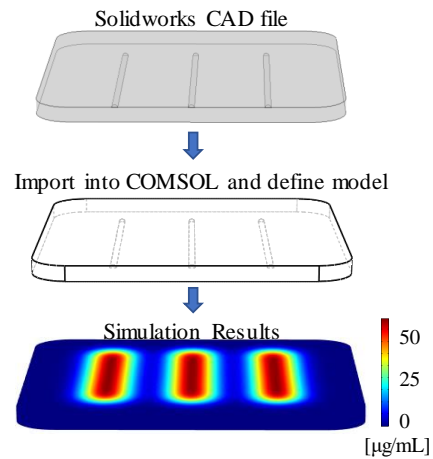


**Figure 5.1. Schematic of COMSOL Simulation Fabrication.** A CAD file is created in SolidWorks and imported into COMSOL, the model is defined and run resulting in a concentration vs time profile.



### 5.2.2 Using a Model to Create a Predictive System

Through experiments it was observed that with the unaided eye this biological system had only two states: a start with no bacterial growth and an end with a distinct inhibition zone, whereas a COMSOL model outputted concentration profiles over time as seen in Figure 5.2.

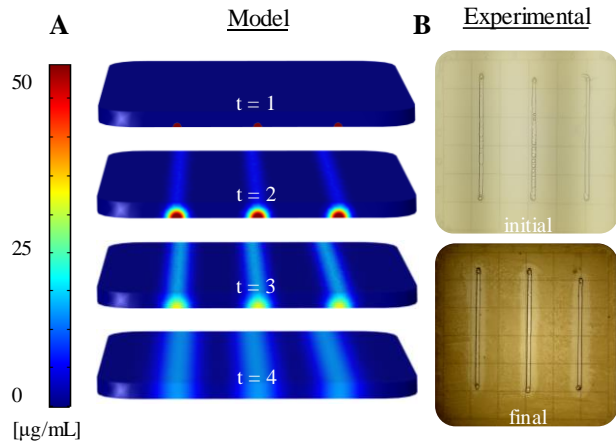


**Figure 5.2. Comparison of COMSOL Theoretical and Experimental Results.** (A) COMSOL output with arbitrary times and (B) initial and final experimental results.

The ultimate goal of this system is to run an experiment with simple vasculature and resultant bacterial patterning, characterize

the system, and create a theoretical model to ultimately predict and control bacteria surface coverage.

This process is depicted in Figure 5.3.

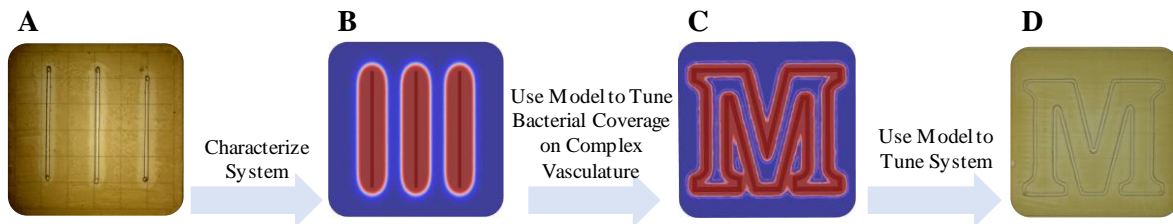


**Figure 5.3. Process of Creating a Predictive System.** (A) Experimental results from simple vasculature are used to create (B) a predictive model, the model is then used to achieve (C) desired bacterial coverage ultimately yielding the (D) desired bacterial coverage on more complex vasculature. Red coloration in the theoretical models indicates zone of inhibition and blue coloring bacterial coverage.

This model contains two distinct processes: diffusion of antibiotics to the biointerface and the growth and uptake of the antibiotics by the bacteria. Modeling the diffusion of antibiotics to the surface, in our case gentamicin sulfate, requires the knowledge of the diffusion coefficient.

This unknown apparent diffusion coefficient was solved for using the COMSOL simulation. Model inputs included an arbitrary diffusion coefficient, antibiotic concentration in channels (20, 40, 50, 60, 80, and

100 ug/mL), and the polymer material initial antibiotic concentration of zero. Experimentally, with each individual starting antibiotic concentration a different inhibition zone was observed. The larger the antibiotic concentration the larger the zone. The surfaces of the agar for all antibiotic concentrations were inoculated with the same number of bacteria at the same time. Here, we assumed that rate of bacterial growth between the concentrations was the same, ultimately resulting in inhibition zones being formed at the same time: the critical time. As stated in Chapter 4, the inhibition zone is formed at the point where the antibiotic concentration equals the minimum inhibitory concentration at the critical time. To summarize, it was assumed that the inhibition zone was formed at the same time (critical time) and concentration (MIC) for all plates regardless of antibiotic concentration in the channels. Knowing all of these parameters the apparent diffusion coefficient, which is expected to be equal for all antibiotic concentrations, was solved for. The graphs used to determine the resultant apparent diffusion coefficient yielding an intersection between the inhibition zone, MIC, and critical time can be seen in Figure 5.4A. The resultant apparent diffusion coefficients can be seen in Figure 5.4B.

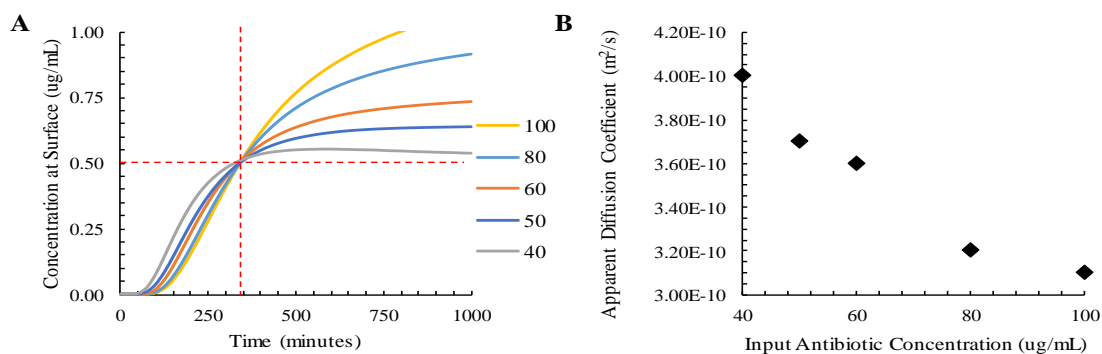


**Figure 5.4. Fitting Apparent Diffusion Coefficient to Inhibition Zone, Critical Time and MIC.** (A) Graph of surface concentration at the inhibition zone versus time used to approach apparent diffusion coefficient (B) apparent diffusion coefficients from fitting parameters.

It can be seen that the resultant apparent diffusion coefficients from the fit varied and that the values decreased as concentration increased. The resultant apparent diffusion coefficients may be attributed to some incorrect assumptions of the model construction. A no flux boundary condition at the surface was assumed. However, as mentioned previously, the antibiotics were not all accumulating at the surface,

some were being consumed by the bacteria. The differing diffusion coefficients may also be attributed to the fact that the diffusion may have been at different stages between concentrations (approaching peak concentration vs equilibrium) at the critical time (Figure 5.5). These hypotheses will need to be further investigated to determine their feasibility.

Theoretical COMSOL models were also run assuming an arbitrary diffusion coefficient of  $5 \times 10^{-10} \text{ m}^2/\text{s}$  for all antibiotic concentrations.

Instead of matching MIC, critical time, and inhibition zone, a new approach was taken. Various time intervals were investigated to determine if the relationship of inhibition zone versus antibiotic concentration was preserved between experiment and theory. Theoretical inhibition zones were standardized using the experimental data from the antibiotic concentration of 50 ug/mL. Standardization was achieved by generating surface concentration versus inhibition zone plots for each antibiotic concentration and marking the inhibition zone achieved by the 50 ug/mL concentration which was 5.7 mm when measuring from the center of the channel rather than the edge. The intersecting surface concentration was then assigned the MIC. Inhibition zone data from the other antibiotic concentrations were determined by locating the intersection of the MIC. These graphs can be seen in Appendix B. The new theoretical inhibition zones were then plotted with the experimental inhibition zone data. Upon indication that the arbitrary theory was following a similar trend to experimental data, more theoretical time points were analyzed to determine the time range at which the theoretical results were within the experimental error (Figure 5.6). It is important to note that each theoretical line at a given time point has a

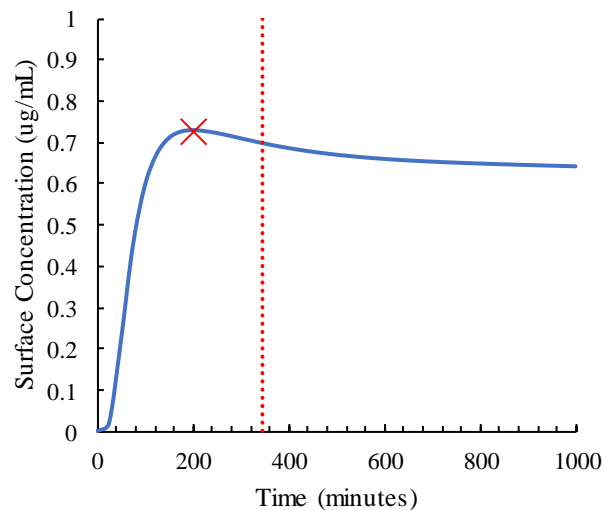


**Figure 5.5 Surface Concentration for 50 ug/mL Antibiotic Concentration.** The red x indicates the time point at which the maximum surface concentration was reached. The dashed line indicates the experimentally determined critical time point.

different MIC. This method resulted in an approximation of both the range of times that fit the experimental error and MICs at which these inhibition zones occur at.

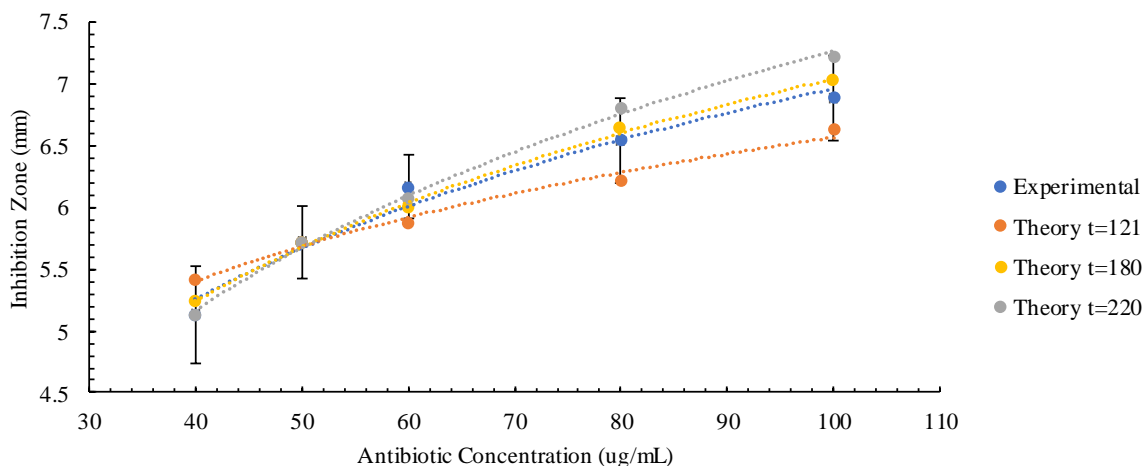


**Figure 5.6 Comparison of Theoretical and Experimental Inhibition Zones.** Time points at which the theory was within the experimental error was determined.

### 5.3 Discussion and Conclusions

Prior to the creation of the model, it was assumed that the diffusion coefficient would be constant for the system regardless of starting antibiotic concentration. However, upon matching a diffusion coefficient to each starting antibiotic concentration by finding the intersection of the inhibition zone, critical time, and MIC, they were different. This result indicated that if a constant diffusion coefficient assumption was true, additional factors must be influencing the results. Initially, it was thought that this difference could be due to the faulty boundary condition assumption of accumulation at the surface and maybe consumption of antibiotics could account for this difference. The same number of bacteria were initially added to each plate, so in order for this theory to prove true, antibiotic flux into the bacteria must be related to the concentration of the antibiotics. The higher the antibiotic concentration, the greater the flux. It is also possible that the flux is negligible compared to the diffusion of antibiotics and is not contributing to this problem at all.

If it was true that flux at the surface was negligible, another explanation could be due to using the faulty critical time parameter as previously discussed in Chapter 4. The actual critical time is most likely shorter than the time calculated experimentally in this research due to the fact that the calculated critical time includes the time it takes the antibiotics to diffuse to the surface as well as the response time of the bacteria themselves. When studying the surface concentration versus time outputs calculated with the arbitrary diffusion coefficient in COMSOL, the possibility that the maximum surface concentration had already occurred and that the system was moving towards equilibrium at the critical time was identified. Meaning that the matching process was identifying the second time at which the surface concentration approaches the MIC and not the first. Further testing and/or model must be conducted to determine the actual cause of the varying diffusion coefficients.

For the second method, the diffusion coefficient was assumed to be the same. The theoretical models were constructed with a constant diffusion coefficient and inhibition zones standardized off of the 50 ug/mL antibiotic concentration experimental trial. This method utilized an arbitrary diffusion coefficient with a goal of determining whether or not a similar relationship between inhibition zone and antibiotic concentration could be observed. It turned out that the trend was very similar to the experimental results. The time range of which the theory was within error was approximately 100 minutes. The results of this arbitrary model were very promising and were an indicator that the bacterial patterning was dominated by the antibiotic diffusion process. However, determination of the apparent diffusion coefficient is necessary in order to truly match this model to experiments.

## CHAPTER 6

### APPLICATIONS OF VASCULARIZED ANTIBIOTIC DELIVERY SYSTEMS

#### 6.1 Introduction

With the imminent consequences of global warming and a continually rising global population, Earth's natural resources are dwindling and the sustainability of human life on Earth as we know it is becoming threatened. With the rapid development of technology for space travels the prospect of Lunar and Martian missions is more promising by day. However, the health risks associated with prolonged travel and limited accessibility to healthcare presents a major threat. Due to the close proximity of individuals traveling in space and the continual recycling of resources, infections are all too common. What start as normal microbial inhabitants of the human body unpredictably mutate into pathogenic, antibiotic resistant organisms capable of threatening the health of passengers.<sup>58-60</sup> To make things worse, the integrity of antibiotics to treat these pathogens is compromised on space missions.<sup>58</sup> In this research, we propose a simple, fast, and cheap solution to identify antibiotic resistance that is able to function in microgravity. This same technology will then be able to be used to create customized treatment plans to combat these opportunistic pathogens on space missions. The system was constructed by strategically placing channels within a typical agar-based cell culture plate using 3D gel printing techniques. The plate was then streaked with a mixed culture of antibiotic resistant microbes and antibiotics inserted into the channels. Using these methods, mixed cultures of bacteria were successfully sorted according to antibiotic resistance and potential mutant colonies isolated for further analysis.

#### 6.2 Materials and Methods

##### 6.2.1 Arbitrary Patterning

Arbitrary patterning of a biointerface can be used to create bacterial cultures of desired shape and size within the millimeter scale using the fabrication methods presented in Chapter 3.

### 6.2.2 Separation According to Antibiotic Resistance

A three-channel vascular pattern was encapsulated into an agar matrix according to the procedures outlined in Chapter 3. *E. coli* GFP and *B. subtilis* stock cultures were individually grown on LB agar plates with 5 ug/mL gentamicin sulfate and 100 ug/mL kanamycin sulfate added, respectively, to select for their antibiotic resistance genotypes. Next, antibiotics were added to the three channels. Equal parts of 30 ug/mL gentamicin sulfate and 300 ug/mL kanamycin sulfate were mixed together and added to the left channel for resulting concentrations of 15 ug/mL gentamicin sulfate and 150 ug/mL kanamycin sulfate. The middle channel was filled with 150 ug/mL kanamycin sulfate and the right channel 15 ug/mL gentamicin sulfate. The plates were left to incubate overnight for 18 to 24 hours at 37 °C.

### 6.2.3 Bacterial Regrowth

A vascular pattern was encapsulated into an agar matrix according to the procedures outlined in Chapter 3. Individual plates were streaked with *E. coli* GFP and *S. epidermidis*. A concentration of 50 ug/mL gentamicin sulfate was added to the *S. epidermidis* streaked plates and 150 ug/mL kanamycin sulfate to the *E. coli* GFP plates. The plates were incubated for 48 hours at 37 °C.

### 6.3 Results

As seen in Figure 6.1, varying degrees and complexity of bacterial surface coverage can be achieved through varying the channel geometry. Figure 6.2. demonstrates the ability to successfully separate bacterial strains of varying antibiotic resistances. The channel on the left

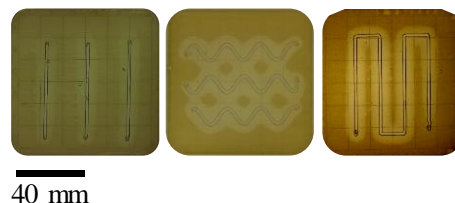


**Figure 6.1. Arbitrary Surface Patterning.**

was treated with a combination of gentamicin sulfate and kanamycin sulfate and resulted in no growth on the surface above the channel. The middle channel was treated with kanamycin sulfate and resulted in isolated growth of *B. subtilis* which carried a gene for kanamycin resistance. The right channel was treated with gentamicin sulfate and resulted in isolated growth of *E. coli* GFP. The isolation of growth was confirmed using quadrant streak plates as well as fluorescence microscopy to detect the presence of

*E. coli* GFP. The regrowth of *S. epidermidis* and *E. coli* GFP following the depletion of antibiotics can be found in figure 6.3.

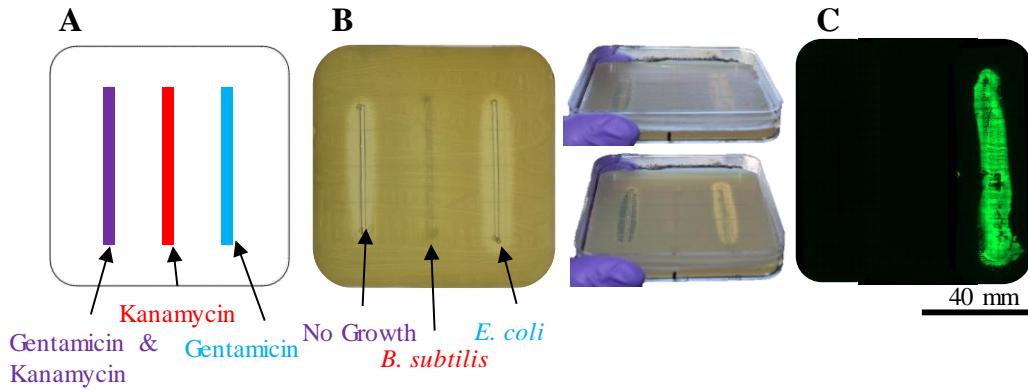


**Figure 6.2. Separation According to Antibiotic Resistance.** A) Agar plate is streaked with a mixture of *E. coli* GFP (gentamicin resistant) and *B. subtilis* (kanamycin resistant). Gentamicin and kanamycin, kanamycin, and gentamicin are added to the channels. B) The isolation of *B. subtilis* was achieved over the kanamycin channel and *E. coli* GFP over the gentamicin channel. No growth was observed over the channel with the combination of antibiotics. C) Fluorescence microscopy was used to verify the isolation of *E. coli* GFP over the gentamicin channel.

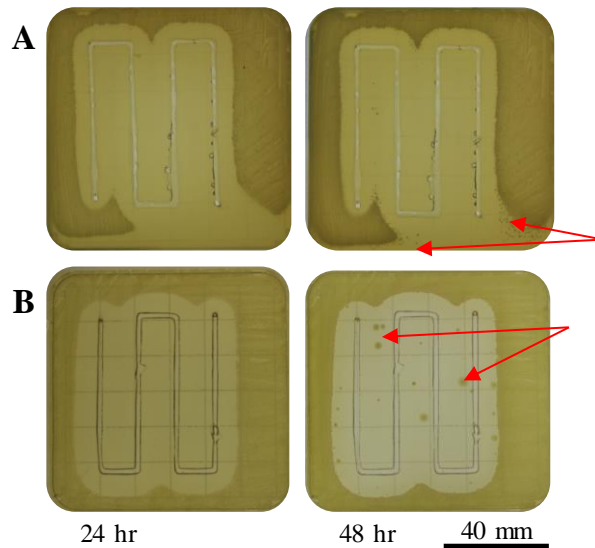


**Figure 6.3. Bacterial Regrowth Following Antibiotic Treatment.** A) *S. epidermidis* and B) *E. coli* GFP. Red arrows indicate areas where regrowth was observed.



## **6.4 Discussion and Conclusions**

The ability to arbitrarily pattern a surface using vascular channels is quite useful and simple. This process occurs passively as the antibiotics are delivered through diffusion. Precisely controlling when and where bacteria grow is key to improving and customizing sample preparation in pursuit of point-of-care diagnostic improvements. It has been demonstrated that through the use of strategic geometry and antibiotic treatments, bacteria can be separated according to possession of antibiotic resistance genes without the use of liquid cultures. As seen in the bacterial regrowth studies, isolated colonies can also be achieved to allow for further characterization. With further testing it can be determined if this regrowth is attributed to the development of antibiotic resistance or if it is an indication of an already present mutation.

In addition to an increase in passenger safety in prolonged space travels, this technology can be directly applied to Earth applications. This technology would be beneficial in other confined and/or isolated spaces where humans inhabit for long periods of time and medical attention may not be readily available, such as Antarctica research stations. This low cost, simple testing platform can also be used in rural areas where diagnostic research labs do not exist.

## CHAPTER 7

### CONCLUSIONS AND FUTURE DIRECTIONS

#### 7.1 Review

This work has resulted in the development of a vascularized bacterial cell culturing platform as a novel development in the field of bacterial patterning, which introduce new ways to manipulate bacterial samples. This work has established methods to construct and perform proof-of-principle tests on vascularized agar bacterial cell culturing systems. Methods for the creation and interpretation of COMSOL models were also developed.

It was shown that arbitrary bacterial surface patterning can be achieved through the insertion of vascular channels within the agar, of which deliver bioactive compounds to the biointerface. The precise three-dimensional positioning of the vascular channels results in the ability to control surface bacterial patterning in both a spatial and temporal manner.

Through characterization of experimental trials with simple vasculature, it was proven possible to create a predictive model of much more complex channel geometries. This model was created in COMSOL using the transport of diluted species module in a time dependent solver. Experimentally determined parameters including inhibition zone, critical time, and MIC were used in the refinement of the model.

The arbitrary bacterial patterning has proven useful in applications of sorting bacteria according to antibiotic resistance. It was also shown that isolated colonies of potential mutants can be achieved.

#### 7.2 Future Directions

The discrepancies between our experimental and published MIC values will need to be further investigated. Experimental results indicate that our MICs are above 1.5 ug/mL. However, theoretical COMSOL models are indicating that a concentration of 1.5 ug/mL is never achieved at the observed inhibition zone. New experiments will need to be constructed to determine the MIC and COMSOL models will need to be reviewed to ensure boundary conditions are being accounted for as expected.

One very interesting avenue that will be pursued in the future is the difference between the inhibition zone of *E. coli* GFP of the unaided eye and the that observed using fluorescence microscopy. Time lapse photos of each system will be used to create a relationship between the two. This will ultimately allow for more information to be extracted about critical time and the timing of the different phases of the bacterial growth curve.

The additional data obtained from the fluorescence inhibition zone studies will contribute to the continued refinement of the COMSOL models. The COMSOL models have been proposed with one currently utilizing an arbitrary apparent diffusion coefficient. However, future work will be necessary to determine which model is more likely. The cause for the differing diffusion coefficients in the first model must be elucidated and for the second model, the appropriate times and diffusion coefficients must be determined.

### **7.3 Summary**

In summary, this work established methods for the creation, characterization, and modeling of bacterial patterning on vascularized polymer platforms. Applications such as customizable sample preparation for point-of-care diagnostics and detection of antibiotic resistance were discussed. This work presented information essential for further development of this platform technology. Potential for this platform technology extends beyond bacterial cell culturing and into applications of localized chemical reactions, wound healing and toxicity assays, and tunable antifouling materials.

## REFERENCES

1. Idota N, Tsukahara T, Sato K, Okano T, Kitamori T. The use of electron beam lithographic graft-polymerization on thermoresponsive polymers for regulating the directionality of cell attachment and detachment. *Biomaterials*. 2009;30(11):2095–101.
2. Nakanishi J, Kikuchi Y, Takarada T, Nakayama H, Yamaguchi K, Maeda M. Spatiotemporal control of cell adhesion on a self-assembled monolayer having a photocleavable protecting group. *Anal Chim Acta*. 2006;578(1):100–4.
3. Niepel MS, Kirchhof K, Menzel M, Heilmann A, Groth T. Control of Cell / Film Interactions Controlling Cell Adhesion Using pH-Modified Polyelectrolyte Multilayer Films. *Layer-by-Layer Film Biomed Appl*. 2015;1–29.
4. Wong JY, Langert R, Ingber DE. Electrically conducting polymers can noninvasively control the shape and growth of mammalian cells. *Proc Natl Acad Sci USA*. 1994;91(April):3201–4.
5. Kiang JD, Wen JH, del Álamo JC, Engler AJ. Dynamic and reversible surface topography influences cell morphology. *J Biomed Mater Res Part A*. 2013 Aug;101A(8):2313–21.
6. Uhrich KE, Cannizzaro SM, Langer RS, Shakesheff KM. Polymeric Systems for Controlled Drug Release. *Chem Rev*. 1999;99:3181–98.
7. Yu S, Zhang X, Tan G, Tian L, Liu D, Liu Y, et al. A novel pH-induced thermosensitive hydrogel composed of carboxymethyl chitosan and poloxamer cross-linked by glutaraldehyde for ophthalmic drug delivery. *Carbohydr Polym*. 2017;155:208–17.
8. Demers CJ, Soundararajan P, Chennampally P, Cox GA, Briscoe J, Collins SD, et al. Development-on-chip: in vitro neural tube patterning with a microfluidic device. *Development*. 2016;143(11):1884–92.
9. Kim S, Kim HJ, Jeon NL. Biological applications of microfluidic gradient devices. *Integr Biol (Camb)*. 2010;2:584–603.
10. Jeon NL, Dertinger SKW, Chiu DT, Choi IS, Stroock AD, Whitesides GM, et al. Generation of Gradients Having Complex Shapes Using Microfluidic Networks Generation of Gradients Having Complex Shapes Using Microfluidic Networks. *Lab Chip*. 2007;7(15):8311–6.
11. Lin F, Saadi W, Rhee SW, Wang S-J, Mittal S, Jeon NL. Generation of dynamic temporal and spatial concentration gradients using microfluidic devices. *Lab Chip*. 2004;4(3):164–7.
12. Hansen CJ, Wu W, Toohey KS, Sottos NR, White SR, Lewis JA. Self-healing materials with interpenetrating microvascular networks. *Adv Mater*. 2009;21(41):4143–7.
13. Howell C, Vu TL, Lin JJ, Kolle S, Juthani N, Watson E, et al. Self-replenishing vascularized fouling-release surfaces. *ACS Appl Mater Interfaces*. 2014;6(15):13299–307.
14. Carmeliet P, Jain RK. Angiogenesis in cancer and other diseases. *Nature*. 2000 Sep;407(6801):249–57.
15. Kirchhoff F, De Pablo Y, Zandén C, Puschmann TB, Pekny M, Pekna M, et al. Bioactive 3D cell culture system minimizes cellular stress and maintains the in vivo -like morphological complexity of astroglial cells. *Glia*. 2013;61(3):432–40.

16. Bertassoni LE, Cecconi M, Manoharan V, Nikkhah M, Hjortnaes J, Cristino AL, et al. Hydrogel bioprinted microchannel networks for vascularization of tissue engineering constructs. *Lab Chip*. 2014;14(13):2202–11.
17. Wu W, Deconinck A, Lewis JA. Omnidirectional printing of 3D microvascular networks. *Adv Mater*. 2011;23(24):178–83.
18. Ee VIKL, Anzi ALML, Go HAN, Oo SECY, Incent PEA V. Generation of Multi-scale Vascular Network System Within 3D Hydrogel Using 3D Bio-printing Technology. 2014;7(3):460–72.
19. Miller JS, Stevens KR, Yang MT, Baker BM, Nguyen DHT, Cohen DM, et al. Rapid casting of patterned vascular networks for perfusable engineered three-dimensional tissues. *Nat Mater*. 2012;11(9):768–74.
20. Paulsen SJ, Miller JS. Tissue vascularization through 3D printing: Will technology bring us flow? *Dev Dyn*. 2015;244(5):629–40.
21. Zhang YS, Arneri A, Bersini S, Shin S-R, Zhu K, Goli-Malekabadi Z, et al. Bioprinting 3D microfibrillar scaffolds for engineering endothelialized myocardium and heart-on-a-chip. *Biomaterials*. 2016;110:45–59.
22. Sun T, Qing G, Su B, Jiang L. Functional biointerface materials inspired from nature. *Chem Soc Rev*. 2011;40(5):2909–21.
23. Briscoe J, Ribes V. Establishing and Interpreting Graded Sonic Hedgehog Signaling during Vertebrate Neural Tube Patterning: The Role of Negative Feedback. *Cold Spring Harb Perspect Biol*. 2009;1(2):a002014–a002014.
24. Kuberski P. Introduction: The complexities of leukocyte recruitment. *Semin Immunol*. 2002;14(2):65–72.
25. Müller A, Homey B, Soto H, Ge N, Catron D, Buchanan ME, et al. Involvement of chemokine receptors in breast cancer metastasis. *Nature*. 2001;410:98–101.
26. Sourjik V, Wingreen NS. Responding to chemical gradients: Bacterial chemotaxis. *Curr Opin Cell Biol*. 2012;24(2):262–8.
27. Chung BG, Flanagan LA, Rhee SW, Schwartz PH, Lee AP, Monuki ES, et al. Human neural stem cell growth and differentiation in a gradient-generating microfluidic device. *Lab Chip*. 2005;5(4):401–6.
28. Toh AGG, Wang ZP, Yang C, Nguyen NT. Engineering microfluidic concentration gradient generators for biological applications. *Microfluid Nanofluidics*. 2014;16(1–2):1–18.
29. Chung BG, Lin F, Jeon NL. A microfluidic multi-injector for gradient generation. *Lab Chip*. 2006;6(6):764–8.
30. Vermes I, Poot AA, van der Meer AD, Vermeul K, Feijen J. A microfluidic wound-healing assay for quantifying endothelial cell migration. *Am J Physiol Circ Physiol*. 2009;298(2):H719–25.
31. Abhyankar V V., Lokuta MA, Huttenlocher A, Beebe DJ. Characterization of a membrane-based gradient generator for use in cell-signaling studies. *Lab Chip*. 2006;6(3):389–93.
32. George SC, Thomas S. Transport phenomena through polymeric systems. *Prog Polym Sci*. 2001;26(6):985–1017.

33. Truskey GA, Yuan F, Katz DF. *Transport Phenomena in Biological Systems*. Second Edi. Upper Saddle River: Pearson; 2009. 888 p.
34. Bird RB (Robert B, Stewart WE, Lightfoot EN. *Transport phenomena*. J. Wiley; 2007. 905 p.
35. Bettini R, Colombo P, Massimo G, Catellani PL, Vitali T. Swelling and drug release in hydrogel matrices: polymer viscosity and matrix porosity effects. *Eur J Pharm Sci*. 1994;2(3):213–9.
36. Colombo P, Bettini R, Santi P, Peppas NA. Swellable matrices for controlled drug delivery: Gel-layer behaviour, mechanisms and optimal performance. *Pharm Sci Technol Today*. 2000;3(6):198–204.
37. Lee PI. Kinetics of drug release from hydrogel matrices. *J Control Release*. 1985;2(C):277–88.
38. Yamamoto M, Ikada Y, Tabata Y. Controlled release of growth factors based on biodegradation of gelatin hydrogel. *J Biomater Sci Polym Ed*. 2001;12(1):77–88.
39. Nestle NFEI, Kimmich R. Concentration-dependent diffusion coefficients and sorption isotherms. Application to ion exchange processes as an example. *J Phys Chem*. 1996;100(30):12569–73.
40. Sia SK, Whitesides GM. Microfluidic devices fabricated in poly(dimethylsiloxane) for biological studies. *Electrophoresis*. 2003;24(21):3563–76.
41. Theriault D, Shepherd RF, White SR, Lewis JA. Fugitive inks for direct-write assembly of three-dimensional microvascular networks. *Adv Mater*. 2005;17(4):395–9.
42. Kolesky DB, Truby RL, Gladman AS, Busbee TA, Homan KA, Lewis JA. 3D bioprinting of vascularized, heterogeneous cell-laden tissue constructs. *Adv Mater*. 2014;26(19):3124–30.
43. Kinstlinger IS, Miller J. 3D-printed Fluidic Networks as Vasculature for Engineered Tissue. *Lab Chip*. 2016;16(3):2025–43.
44. Murphy S V, Atala A. 3D bioprinting of tissues and organs. *Nat Biotechnol*. 2014;32(8):773–85.
45. Golden AP, Tien J. Fabrication of microfluidic hydrogels using molded gelatin as a sacrificial element. *Lab Chip*. 2007;7(6):720.
46. Zhu W, Ma X, Gou M, Mei D, Zhang K, Chen S. 3D printing of functional biomaterials for tissue engineering. *Curr Opin Biotechnol*. 2016;40:103–12.
47. Cole MA, Voelcker NH, Thissen H, Griesser HJ. Stimuli-responsive interfaces and systems for the control of protein-surface and cell-surface interactions. *Biomaterials*. 2009;30(9):1827–50.
48. Recht MI, Fourmy D, Blanchard SC, Dahlquist KD, Puglisi JD. RNA sequence determinants for aminoglycoside binding to an A-site rRNA model oligonucleotide. *J Mol Biol*. 1996;262(4):421–36.
49. Taber, Harry W., Mueller, John P., Miller, Paul F., Arrow AS. Bacterial uptake of aminoglycoside antibiotics. *Microbiol Rev*. 1987;51(4):439–57.
50. Fujikawa H, Morozumi S. Modeling Surface Growth of *Escherichia coli* on Agar Plates. *Appl Environ Microbiol*. 2007 Apr 1;73(7):2404–2404.
51. CLSI. *Performance Standards for Antimicrobial Disk Susceptibility Tests; Approved Standard—Twelfth Edition*. CLSI document M02-A12. Wayne, PA: Clinical and Laboratory Standards Institute; 2015.

52. CLSI. Performance Standards for Antimicrobial Susceptibility Testing. 27th ed. CLSI supplement M100. Wayne, PA: Clinical and Laboratory Standards Institute; 2017
53. Wiegand I, Hilpert K, Hancock REW. Agar and broth dilution methods to determine the minimal inhibitory concentration (MIC) of antimicrobial substances. *Nat Protoc.* 2008;3(2):163–75.
54. Cooper KE, Woodman D. The diffusion of antiseptics through agar gels, with special reference to the agar cup assay method of estimating the activity of penicillin. *J Pathol Bacteriol.* 1946;58(1):75–84.
55. Hasselmann C, Diseases I. Determination of minimum inhibitory concentrations (MICs) of antibacterial agents by broth dilution. *Clin Microbiol Infect.* 2003;9(8):ix–xv.
56. Hudzicki J. Kirby-Bauer disk diffusion susceptibility test protocol. American Society for Microbiology. 2009.
57. Cavenaghi LA, Biganzoli E, Danese A, Parenti F. Diffusion of teicoplanin and vancomycin in agar. *Diagn Microbiol Infect Dis.* 1992;15(3):253–8.
58. Taylor PW. Impact of space flight on bacterial virulence and antibiotic susceptibility. *Infect Drug Resist.* 2015;8:249–62.
59. Crabbé A, Schurr MJ, Monsieurs P, Morici L, Schurr J, Wilson JW, et al. Transcriptional and proteomic responses of *Pseudomonas aeruginosa* PAO1 to spaceflight conditions involve Hfq regulation and reveal a role for oxygen. *Appl Environ Microbiol.* 2011;77(4):1221–30.
60. Lapchine L, Moatti N, Gasset G, Richoilley G, Templier J, Tixador R. Antibiotic activity in space. *Drugs Exp Clin Res.* 1986;12(12):933–8.

## APPENDIX A. VASCULAR CHANNEL CHARACTERIZATION RAW DATA

Chapter 4 reported methods of characterizing the bacterial surface patterning parameters of inhibition zone, MIC, and critical time. Table A.1. shows the raw inhibition zone measurements for both *S. epidermidis* and *E. coli* K12. Table A.2. shows the raw data for the MIC experimental trials, and Table A.3. the data from the critical time trials. Inhibition zone measurements from the evaporation studies are also included in Table A.4.

**Table A.1. Inhibition Zone Raw Data.** Measured immediately following 18 to 24 hour incubation period.

Inhibition Zone (mm)						
<i>S. epidermidis</i>						
Antibiotic Concentration (µg/mL)						
Trial	40	50	60	80	100	
1	4.78	--	5.57	5.79	6.18	
2	4.39	5.57	5.40	5.95	--	
3	3.83	5.71	4.91	5.23	5.57	
4	4.35	5.35	5.85	6.68	7.22	
Average	4.34	5.54	5.43	5.91	6.32	
Standard Deviation	0.39	0.18	0.40	0.60	0.83	
<i>E. coli</i> K12						
Antibiotic Concentration (µg/mL)						
Trial	40	50	60	80	100	
1	--	4.62	--	--	5.87	
2	4.83		5.01	5.57	5.62	
3	4.42	4.73	5.16	5.90	--	
4	4.05	4.68	5.69	5.57	5.77	
5	3.81	5.26	5.15	5.29	6.50	
6	4.06	--	5.30	5.88	6.15	
Average	4.23	4.82	5.26	5.64	5.98	
Standard Deviation	0.69	0.52	0.46	0.34	0.35	



**Table A.2. Minimum Inhibitory Concentration Agar Plate Method Raw Data.** Results indicate colony forming unit (CFU) counts and CG indicates confluent growth and inability to distinguish between number of CFUs. The hyphen indicates that no trial was performed at the specified antibiotic concentration.

<i>S. epidermidis</i>												
Antibiotic Concentration (ug/mL)												
Trial	0.5	1	1.5	2	2.5	3	4	5	6	7	10	50
1	CG	CG	CG	CG	CG	-	-	-	-	-	-	-
2	CG	CG	CG	CG	CG	-	-	-	-	-	-	-
3	CG	CG	CG	CG	CG	-	-	-	-	-	-	-
4	-	-	-	-	-	1	5	0	0	0	-	-
5	-	-	-	-	-	67	18	4	6	6	-	-
6	-	-	-	-	-	67	18	34	12	9	-	-
7	-	-	-	-	-	0	0	0	0	0	-	-
8	-	-	-	-	-	4	0	0	0	0	-	-
9	-	100	-	-	-	-	-	0	-	-	0	0

<i>E. coli K12</i>											
Antibiotic Concentration (ug/mL)											
Trial	1	2	3	4	5	6	7	7.5	8	10	50
1	CG	CG	52	16	3	-	-	-	-	-	-
2	CG	CG	41	17	8	-	-	-	-	-	-
3	CG	CG	48	19	5	-	-	-	-	-	-
4	-	-	6	1	0	0	0	-	-	-	-
5	CG	-	-	-	-	-	-	-	-	4	0
6	CG	-	-	-	25	-	-	-	-	10	0
7	-	-	-	-	11	-	-	2	-	1	-
8	-	-	-	-	16	5	4	-	2	-	-

**Table A.3. Critical Time Data.** Critical times in minutes for *S. epidermidis* and *E. coli* wt.

Trial	<i>S. epidermidis</i>		<i>E. coli</i> K12	
	Critical Time	Sample Size	Critical Time	Sample Size
1	365	8	382	8
2	285	8	377	8
3	420	8	341	9
4	359	9	326	5
5	388	5	293	5
Average	363.4		343.8	
Standard Deviation	49.9		37.0	

**Table A.4. Mann-Whitney U-Test.** A comparison of channel treatments. 2G indicates grease sealing both inlet and outlet, 1G indicates sealing one, and 0G none.

Mann-Whitney U-Test Results	
Null Hypothesis	$H_0: \eta_1 - \eta_2 = 0$
Alternative Hypothesis	$H_1: \eta_1 - \eta_2 \neq 0$
Comparison	P-Value
0G, 1G	0.353
0G, 2G	0.376
1G, 2G	0.174

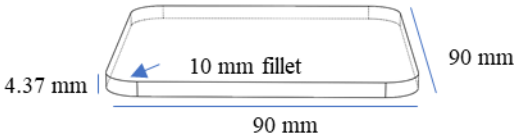
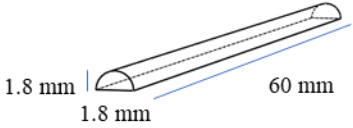
**Table A.5. Evaporation Data.** 0G indicates no grease, 1G indicates one inlet sealed with grease, and 2G indicates both inlet and outlet sealed with grease.

Trial	Inhibition Zone (mm)								
	1			2			3		
Treatment	0G	1G	2G	0G	1G	2G	0G	1G	2G
	5.84	4.50	3.93	4.33	4.47	4.58	4.95	4.29	3.71
	4.83	3.93	3.83	4.59	4.36	3.80	4.15	4.40	4.04
	4.94	4.04	3.82	4.47	4.47	3.92	4.83	4.94	4.72
	4.61	3.93	3.82	4.92	4.47	4.25	4.72	4.72	4.94
	4.72	4.28	3.15	4.80	4.58	3.35	4.95	5.05	3.60
	4.72	4.27	4.27	4.26	4.13	3.58	4.83	4.94	4.50
	4.84	4.39	4.05	4.95	4.70	3.58	4.72	4.94	4.38
	4.83	3.82	3.62	5.47	4.81	3.69	4.15	5.05	3.82
	4.61	4.38	4.16	4.81	4.81	2.91	4.72	4.95	3.93
	4.27	4.49	3.49	4.58	4.02	4.02	4.49	4.17	3.48
	4.61	4.84	4.51	4.36	5.81	4.36	4.49	4.83	5.05
	4.05	4.84	4.73	5.14	5.71	4.81	4.27	5.61	5.39
	4.61	4.38	4.83	5.03	5.93	5.25	3.93	4.94	5.28
	4.05	4.72	5.07	4.59	5.26	5.03	3.93	4.83	5.40
	4.27	4.84	5.06	4.47	4.81	4.82	4.27	4.72	5.17
	4.61	3.94	5.17	5.03	4.81	5.26	4.16	5.28	4.49
	4.16	4.39	5.06	5.36	5.03	5.48	4.40	5.73	4.95
	4.61	4.38	4.95	5.48	4.70	5.92	4.28	4.64	4.94
	4.27	4.49	5.17	5.36	4.47	4.93	4.27	4.60	5.19
	4.04	4.84	5.06	5.03	4.92	4.69	4.27	5.17	4.72
Mean	4.57	4.38	4.39	4.85	4.81	4.41	4.44	4.89	4.59
Median	4.61	4.39	4.39	4.86	4.75	4.47	4.34	4.94	4.72

## APPENDIX B. THEORETICAL MODELING

Chapter 5 presented two possible theoretical models that were matched to experimental results. Table B.1. displays the parameters used in designing the COMSOL theoretical models. The second theoretical model inputted a constant diffusion coefficient of  $5 \times 10^{-10} \text{ m}^2/\text{s}$  for antibiotic concentrations. Theoretical inhibition zones were generated by standardizing with the inhibition zone of 50 ug/mL antibiotic concentration. Figures B.1-3. Display the process of determining the theoretical inhibition zones. For these figures it is important to note that rather than a smooth plot, knees are present around 6 and 7.75 mm due to the resolution of the solver, solutions were generated at 25-minute increments.

**Table B.1. COMSOL Model Parameters.**

COMSOL Model Parameters	
<b>Physics</b>	Transport of Diluted Species
<b>Study</b>	Time Dependent
<b>Mesh Size</b>	Extremely Fine
<b>Geometry</b>	<p><b>Agar</b>            90 mm width            90 mm length            4.37 mm height            10 mm fillet</p> 
	<p><b>Channel</b>            Semicircle            0.9 mm radius</p> 
<b>Governing Equations</b>	$\frac{\partial c_i}{\partial t} + \nabla \cdot (-D_i \nabla c_i) = R_i$ $\mathbf{N}_i = -D_i \nabla c_i$
<b>Boundary Conditions</b>	No flux at exterior agar boundaries: $-\mathbf{n} \cdot \mathbf{N}_i = 0$

$c_i$  = species concentration (mol/m<sup>3</sup>)  
 $t$  = time (s)  
 $D$  = diffusion coefficient (m<sup>2</sup>/s)  
 $R_i$  = production or consumption rate expression  
 $\mathbf{N}_i$  = flux  
 $\mathbf{n}$  = outward unit normal vector

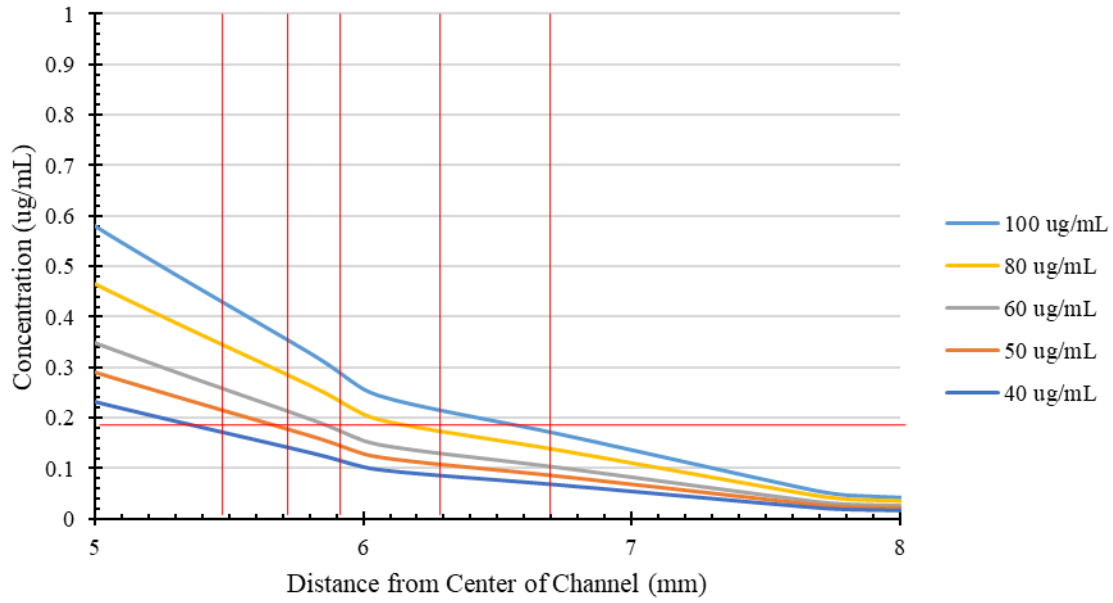


**Figure B.1. Standardized Theoretical Inhibition Zones.** The lower boundary of error where time equals 121 minutes is displayed.

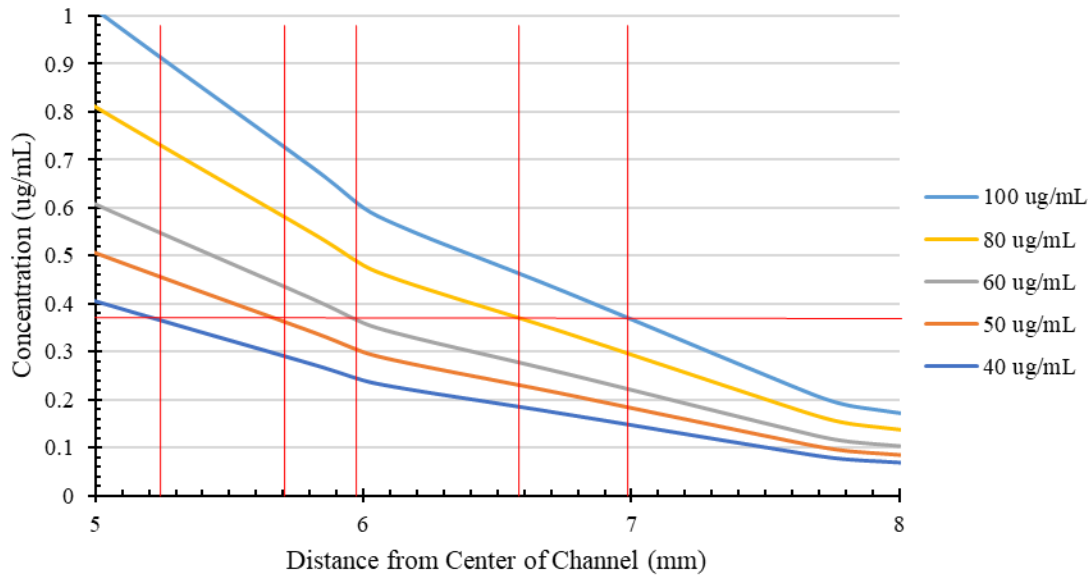


**Figure B.2. Standardized Theoretical Inhibition Zones.** Time equals 180 minutes is displayed.

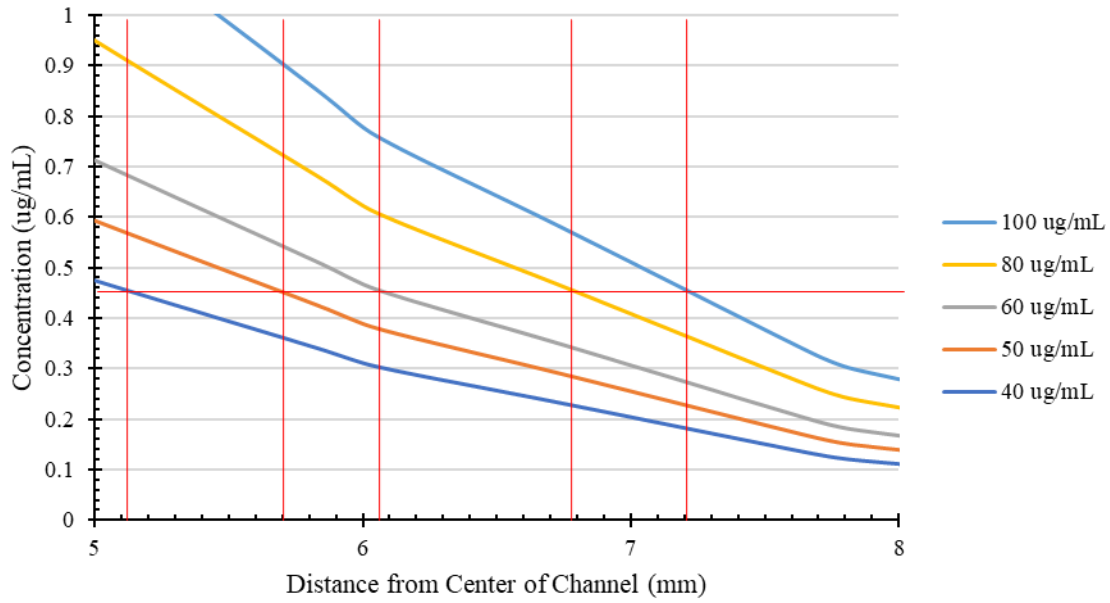


**Figure B.3. Standardized Theoretical Inhibition Zones.** The upper boundary of error where time equals 220 minutes is displayed.

## **BIOGRAPHY OF THE AUTHOR**

Kayla Marquis was born in Bangor, Maine in October of 1994. She was raised in Orono, Maine and graduated from Orono High School in 2013. She went on to receive her Bachelor of Science in Bioengineering with a minor in pre-medical studies from the University of Maine in 2017. Kayla was a member of the University of Maine Track and Field Team throughout her undergraduate career. She worked as a research assistant to Dr. Caitlin Howell during her final undergraduate year. After graduation, Kayla will be pursuing a career in industry. Kayla is a candidate for the Master of Science degree in Biomedical Engineering from the University of Maine in May 2019.